Amphiphilic cyclodextrins: Dimerization and diazepam binding explored by molecular dynamics simulations

Dimas Suárez, Natalia Díaz *

Universidad de Oviedo, Dpto. Química Física y Analítica, C/ Julián Clavería 8, 33006 Oviedo, Asturias, Spain

ARTICLE INFO

ABSTRACT

Amphiphilic cyclodextrins spontaneously aggregate to form different supramolecular assemblies with potential applications in drug release. Herein, we employ extended molecular dynamics simulations in order to characterize the structure and dynamics in explicit solvent of several amphiphilic derivatives of the β-cyclodextrin (β-CD) molecule, with aliphatic chains ester-bound to the wide rim of the hydrophobic cavity. We also study the binding properties considering a typical guest (diazepam) and the dimerization of these macrocyclic systems, assessing the relative stability of the complexes by means of end-point free energy methods. Different lengths (C_4, C_{10}, and C_{14} atoms) are considered for the alkyl side chains included in the amphiphilic β-CD-C_n molecules. According to the simulations, the length of these C_n moieties determines the complexing and aggregation capabilities of the β-CD-C_n systems. Compared to the native β-CD, the alkyl side chains in the β-CD-C_n molecules destabilize the inclusion complexes with diazepam and hinder the access of guest molecules to the hydrophobic cavity. In turn, dimerization is favored in the largest amphiphilic derivatives associated to the hydrophobic interaction between the C_n fragments.

1. Introduction

Cyclodextrins (CDs) are cyclic oligosaccharides formed by a variable number of α-D-glucopyranose units connected by α(1–4) glycosidic linkages [1]. The natural or native molecules comprise α-CD, β-CD, and γ-CD with six, seven, and eight sugar units, respectively. In the solid state, CDs resemble a truncated cone with a central hydrophobic cavity lined by the hydrophilic hydroxyl groups [2]. The secondary alcohols bound to C2 and C3 (see Scheme 1) delimit the wide rim or wide entrance to the cavity (also termed secondary side or head), while primary alcohols in C6 outline the narrow edge (the primary side or tail). Intramolecular hydrogen-bonds between the secondary hydroxyl groups of adjacent sugar rings are supposed to stabilize the conical conformation observed in the crystal structures. However, in solution, CDs are flexible molecules that display distorted toroidal conformations. This flexibility partly arises from the rotation around the glucosidic links that allows the tilting inwards of one or several glucose rings [3,4].

CD molecules present unique binding properties that explain their multiple applications. They are used as complexing agents to stabilize and protect sensitive substances, and to mask pigments or ill smell and taste compounds [5]. In the pharmaceutical industry, CDs are employed to improve the solubility, bioavailability, and stability of drugs [6]. In these applications, CDs are assumed to form inclusion complexes with partially hydrophobic molecules, where the whole guest molecule or some part of it is placed within the inner hydrophobic cavity of the host [7]. CDs also form non-inclusion complexes with other molecules mainly linked to the presence of aggregates, which result from the self-association of several CD units [8,9].

CD aggregation in solution has been invoked to explain some thermodynamic properties, like the abnormally-low solubility values of β-CD presumably due to the unfavorable interaction of the aggregates with the hydrogen bond network of bulk water [10]. According to light scattering and cryo-TEM experiments, β-CD monomers aggregate in water at room temperature in differently-shaped particles (60.0–120.0 nm in size) with critical aggregation concentrations well below its solubility limit [11,12], the extent of aggregation increasing with CD concentration and being enhanced upon inclusion complex formation [13]. Potential of mean force (PMF) calculations for the complexation of two β-CD monomers have also shown that the geometry and stability of the dimer are affected by solvent and influenced by the presence of a guest bound within the central cavity. [14] However, it has been also noticed that, although dynamic light scattering by aggre-

---

* Corresponding author.
*E-mail address:* diazfnatalia@uniovi.es (N. Díaz).
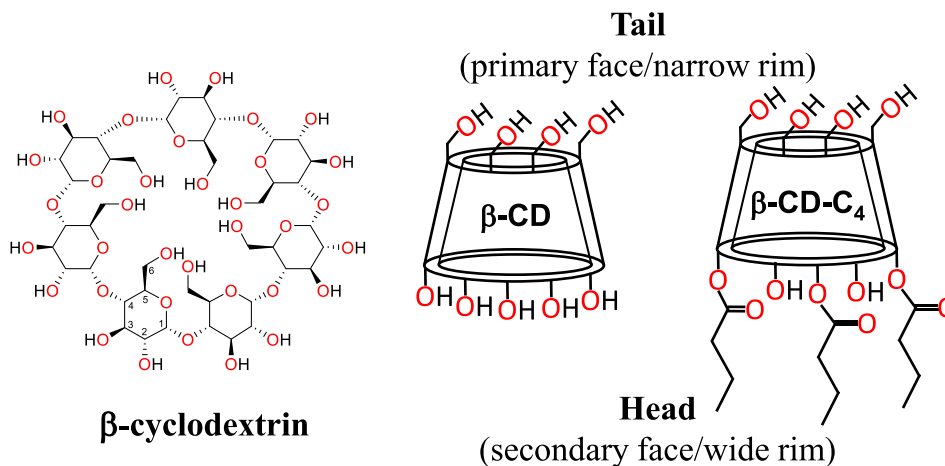
Scheme 1. Schematic representation of β-CD and β-CD-C$_4$.

gates of natural CDs is intense, their molar fraction in solution would be residual when compared to that of free CDs (*e.g.*, 0.0002% for 10 *mM* β-CD at 25 °C) [15]. Similarly, different nuclear magnetic resonance (NMR) experiments have ruled out the presence of well-defined dimers or aggregates for α, β, and γ-CD [16,17], and established a upper limit for their abundance (less than1%). Therefore, the actual stability, structure and relevance of the dimer and/or larger aggregates of the most common natural CDs are still a matter of debate.

The properties of natural CDs can be improved by introducing different substitutions at the exposed primary and secondary alcohols of the glucosyl units. For instance, the unfavorable low aqueous solubility and high nephrotoxicity observed for β-CD are effectively overcome in the hydroxypropyl-β-CD derivative [7]. However, these chemically modified CDs often present mixtures of positional and regional isomers with a variable degree of substitution depending on the reaction conditions. The amphiphilic derivatives (CD-C$_n$) are obtained by grafting aliphatic chains of variable length (C$_n$) on the primary/secondary face of the glucopyranose units of parent CDs by means of different bond types (ester, ether, or amide). These amphiphilic CDs present better interactions with biological membranes than the native CDs [18]. In addition, guess molecules can be included in the CD-C$_n$ cavity or entrapped within their long aliphatic chains. The later has been confirmed in NMR experiments showing that the chemical shifts of the protons located within the β-CD-C$_6$ cavity remained unaltered during progesterone binding [19].

A remarkable feature of amphiphilic CDs is that they spontaneously aggregate to form different supramolecular assemblies. For example, β-CD-C$_n$ nanoparticle suspensions have been prepared with concentrations as low as 1.5 *mg/mL*. [20] The structure of these β-CD-C$_n$ aggregates depends on the chemical nature of the grafted chains, the location of the substitution, the chain length, and the degree of substitution [20,21]. Concerning the binding capabilities of these self-assembled structures, nanoparticles formed by β-CD-C$_{10}$ molecules have been observed to entrap drugs like diazepam (Dzp), a benzodiazepine drug with anxiolytic properties that is widely used for treating epilepsy, insomnia, and anxiety. Actually, diazepam is highly insoluble in water but its bioavailability can be improved by cyclodextrin complexation [22,23]. It forms relatively-stable 1:1 complexes with β-CD (ΔG = −5.7 kcal/mol) [24,25], in which the unsubstituted phenyl ring (Phe in Scheme 2) predominantly resides within the β-CD cavity according to NMR and modelling results [26]. Diazepam binding to β-CD-C$_{10}$ aggregates occurs with a slight increase in the size of the particles, what suggests that Dzp is at least partly
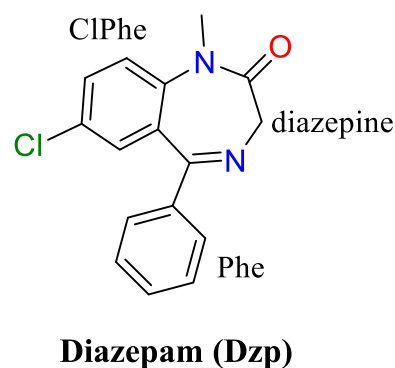
Diazepam (Dzp)

Scheme 2. 2D structure of diazepam.

adsorbed on the nanoparticle surface. [27] However, release experiments have pointed out that some drug molecules would be also located within the nanostructures.

Herein, we aim to carry out a computational study of (a) the complexing capability of β-CD and of three different amphiphilic esterified derivatives (*i.e.*, β-CD-C$_4$, β-CD-C$_{10}$, and β-CD-C$_{14}$) for diazepam to shed light on the role played by the grafted aliphatic chains on guest binding; (b) the structure and stability of the dimer complexes of the same CDs to provide some evidence of their ability to form larger aggregates. The computational approach pursued in this work is based on the experience gained in previous theoretical works showing that long molecular dynamics (MD) simulations in the μs range performed in explicit solvent, and the inclusion of both enthalpic and entropic reorganization effects are essential issues to obtain a good agreement between experimental and computed data [28–34]. Thus, after some parametrization work, the dynamics of the selected β-CD-C$_n$ molecules is sampled by means of 5.0 μs-long MD simulations and the results compared to those previously obtained for the native β-CD [4]. In this way, the influence of the aliphatic chains on the structure and dynamics of the CD macrocycle can be revealed. A series of MD simulations of various complexes formed with diazepam allow us to examine the stability of different inclusion complexes and the formation of alternative non-inclusion compounds. Finally, we explore the ability of β-CD and the three selected β-CD-C$_n$ derivatives to form homodimers considering two different initial arrangements, head-to-head and tail-to-tail. Overall, the computational results provide new insight into the preferred binding modes

that may be useful in future studies of the spontaneous self-aggregation that characterizes the amphiphilic CDs.

2. Methods

2.1. β-CD-C_n parameterization

Initial coordinates for β-CD were obtained from the Cambridge Structural Database (structure 1107195) [35]. For the amphiphilic β-CD-C_n molecules, O2 alcohol groups in β-CD (see Scheme 1) were replaced by ester-bound C_4, C_{10}, and C_{14} alkyl chains (*i.e.* O-CO-$(CH_2)_2$-CH_3, O-CO-$(CH_2)_8$-CH_3, and O-CO-$(CH_2)_{12}$-CH_3) using the tLEaP program included in the AMBER18 package [36,37]. Alkylation at the seven O2 positions was selected according to previous results showing that thermolysin esterification of native β-CD preferentially occurs at that secondary alcohol [38], and that the most intense signal in matrix-assisted laser desorption/ionization mass spectroscopy (MALDI-MS) analysis of the β-CD-C_4, β-CD-C_{10} and β-CD-C_{14} derivatives corresponds to the seven substituted species [39].

We employed the Gaussian09 package [40] to obtain the molecular geometry and the electrostatic potential of the C_4, C_{10}, and C_{14} acylated glucose units capped with –OCH_3 and –CH_3 groups at C1 and O4, respectively. We chose the *ab initio* protocol that is recommended for parameter derivation in the AMBER18 package that combines the Hartree-Fock (HF) method with the double-ζ 6-31G* basis set [41]. The *Gaussian09* output files were processed with the antechamber program included in the AMBER18 package [36] to build new residue representations for the esterified glucose rings taking the atom types and charges for the glucose ring from the GLYCAM-06j force field [42]. Atomic charges for the O2 ester group and the alkyl side chains were computed by charge fitting to the HF/6-31G* electrostatic potential using the Restrained Electrostatic Potential (RESP) methodology [43]. During the RESP calculations, the total charge in the ester moiety was restrained to fit the charge of the O2 alcohol group in the GLYCAM-06j parametrization of the glucose unit.

2.2. Diazepam parameterization

Starting with the X-ray coordinates of diazepam (Dzp) [44], the internal geometry was relaxed at the HF/6-31G* level of theory. Using again antechamber, we assigned GAFF atom types [45] and atomic charges for Dzp, which were built with the RESP methodology and taking into account the HF/6-31G* electrostatic potential. The Dzp ring adopts a boat conformation, which can interconvert into its mirror image through a ring inversion process that has a relatively high-energy barrier. To reproduce such barrier, we refined all the dihedral and implicit torsion parameters involving the Dzp ring atoms using the paramfit program [46] included in AMBER18. To this end, we computed first the conformational path connecting the two conformers by means of the Nudge-Elastic-Band (NEB) method [47] as implemented in the ORCA package [48]. The NEB pathway comprised 14 intermediate (nudge) structures and was optimized using a density-functional-theory (DFT) method that combines the popular B3LYP functional with a large triple-ζ basis set (cc-pVTZ), including also the Grimme dispersion correction (D3)[49] with the Becke-Johnson damping function. Subsequently, the energy profile was refined by means of single-point RI-MP2/aug-cc-pVTZ calculations on the NEB structures. This *ab initio* level of theory, which usually provides accurate conformational energies, gives an energy barrier of 17.9 kcal/mol in good agreement with experimental data and former theoretical calculations [50]. The resulting energies and geometries were introduced

into paramfit, which reoptimized the dihedral parameters applying a least-squares fitting procedure.

2.3. Building of inclusion complexes

Models for the β-CD/Dzp inclusion complexes were generated by considering different arrangements between the diazepam molecule and the selected cyclodextrin. The size of the diazepam molecule makes it impossible to place the whole guest within the β-CD cavity, and only the phenyl ring or a part of the benzodiazepine moiety (Phe and ClPhe in Scheme 2) was considered to be inserted into the host. In addition, the binding of diazepam would occur through the wide rim or head (H), or through the narrow entrance or tail (T). As a result, four different models were initially built and simulated for the β-CD/Dzp inclusion complex (see β-CD/Dzp$_{(Phe-H)}$, β-CD/Dzp$_{(Phe-T)}$, β-CD/Dzp$_{(ClPhe-H)}$, β-CD/Dzp$_{(ClPhe-T)}$ in Scheme 3). However only the two arrangements with the phenyl ring bound within the β-CD cavity remained stable, in agreement with previous results [26]. Thus, initial models for the inclusion complexes formed between the amphiphilic β-CD-C_n and diazepam were only generated by placing the unsubstituted phenyl ring of the guest inside the host cavity. We considered that binding may occur either through the tail (β-CD-C_n/Dzp$_{(T)}$) or through the acylated head entrance of the host (β-CD-C_n/Dzp$_{(H)}$). Initial coordinates for the different β-CD/Dzp complexes were obtained by superposing the center-of-mass of the two molecules and aligning their principal axes of inertia.

2.4. Building of the β-CD dimers

As a first step in the modeling of cyclodextrin aggregation, we considered homodimers formed by two units of β-CD or two units of the amphiphilic derivatives β-CD-C_4, β-CD-C_{10}, and β-CD-C_{14}. For these dimers, two arrangements were built that result from orienting the monomers to interact thought the wide opening (head-to-head, HH) or through the narrow rim (tail-to-tail, TT) of the cyclodextrin ring. Initial coordinates for the different dimers (β-CD/β-CD$_{(HH)}$, β-CD/β-CD$_{(TT)}$, β-CD-C_4/β-CD-$C_{4(HH)}$, etc.) were obtained by rotating/translating one monomer with respect to the other, using the tLEaP program and the parametrization previously developed for the amphiphilic β-CD-C_n derivatives.

2.5. Molecular dynamics settings

The conformational phase space of the examined systems was intensively explore by means of MD simulations in explicit solvent. Each CD molecule, CD/Dzp complex or CD/CD aggregate was placed within an octahedral box of TIP3P water molecules that extended at least 14 Å from the solute atoms [51]. Table S1 collects the size of the equilibrated solvent box and the number of water molecules contained in the different systems. Periodic boundary conditions were applied to simulate continuous systems [52] and long-range interactions were described by the Particle-Mesh-Ewald method [53] with a grid spacing of ∼ 1 Å and a non-bonded cutoff of 9 Å. Water molecules were relaxed by means of energy minimizations and 100 ps of MD at 300 K with the sander program in AMBER18. The full systems were minimized and heated gradually to 300 K during 60 ps of MD (constant NVT) with a time step of 1.0 fs. Subsequently, the systems were pressurized (1 bar) by running a 20.0 ns NPT simulation. During the MD simulations, Langevin dynamics was employed to control the temperature with a collision frequency of 2 ps^{-1} and the length of all R-H bonds was constrained with the SHAKE algorithm. In the NPT run, the pressure of the system was controlled by a Monte Carlo barostat as implemented in AMBER18 [36].
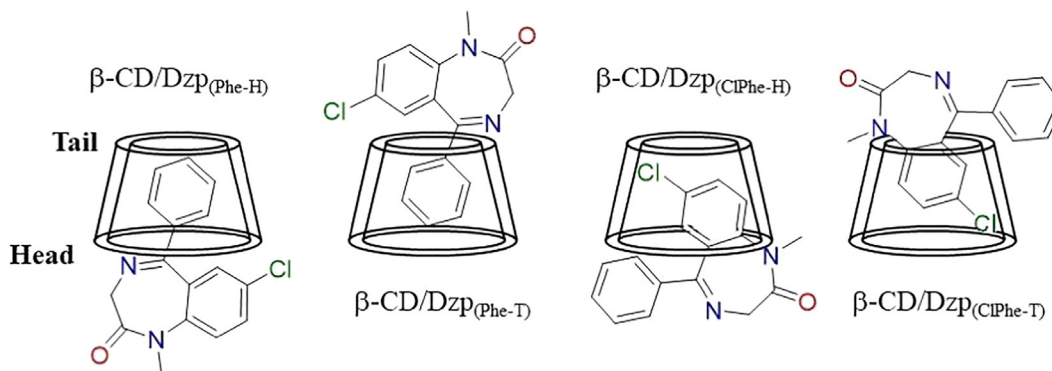
Scheme 3. Binding modes explored for the inclusion complexes between β-CD and Dzp.

The production phase of the simulations comprised 5.0 μs, which were run at NVT conditions with a time step of 2 fs and using the accelerated version of the pmemd code for Graphical Processing Units [54,55]. Coordinates of the solute atoms were saved for analysis every 2.5 ps and those of the solvated systems every 50 ps. For the unbound state of β-CD, we collected MD snapshots from our previous simulation work [4] on the conformational and entropic properties of α-, β- and γ-CDs, which were run for 5.0 μs and using comparable MD settings. Structural analyses were performed using the cpptraj module of AMBER18 [56]. The coordinates of the β-CD atoms along the MD trajectories were clustered using cpptraj with the average-linkage clustering algorithm and a sieve of 50 frames. The distance metric between frames was calculated via best-fit coordinate root mean square deviation (RMSD) using the two ether oxygens (O4 and O5) and the five carbon atoms (C1-C5) in the sugar rings, and the clustering was finished when the minimum distance between clusters was greater than 1.5 Å. The solvent-accessible surface area (SASA) of the CD molecules and their fragment contributions were computed using the linear combination of pairwise overlaps (LCPO) method [57], as implemented in cpptraj. The SASA, which measures the extent to which solute atoms can form contacts with solvent, represents the locus of the center of a spherical solvent molecule (1.4 Å radius) as it rolls over the van der Waals (vdW) spheres placed at the solute atoms with Bondi radii. The Chimera visualization system was employed to draw selected models [58].

To quantify the width of the CD cavity, we computed the radius of accessibility (r_{acc}), which is defined as the maximum radius of a spherical ligand that can touch a set of auxiliary spheres tightly packed in an octagonal disposition and located at the center of mass of the CD ring [4]. For the r_{acc} calculations, we used the MSMS program [59] to carry out fast computations of the molecular surface and a Fortran program developed in house as described in previous work [60].

2.6. Energetic analysis of the MD trajectories

In a previous work, we have studied the performance of different end-point free energy methodologies as applied to β-CD/guest complexes [33]. Thus, in the present work, we estimated the relative stability of the various CD complexes using the protocol that showed the best performance, which employs a semiempirical quantum mechanical (QM) method to estimate the intrinsic stability of solute molecules and their non-covalent complexes taking into account electronic effects like polarization and charge-transfer. The selected QM method provides also atomic charges suitable to evaluate the electrostatic contributions to the solvation Gibbs energy using a solvent continuum model. In particular, we resorted to the DFTB3 version of the self-consistent charges density

functional tight-binding (SCC-DFTB) method [61,62], which is a semiempirical QM method based on a second-order expansion of the DFT total energy around a reference density. The DFTB3 Hamiltonian is expressed in terms of the so-called Slater-Koster parameters, whose values were selected from the 3OB set, specifically optimized for biomolecular calculations [63,64]. In addition, the DFTB3 energy (E_{DFTB3}) was augmented with a solvation energy term which, in turn, comprises an electrostatic Poisson-Boltzmann (PB) solvation energy ($\Delta_{solv}G^{PB}_{elec}$) as well as a non-polar term $\Delta_{solv}G^{SA}_{non-polar}$ (solute-solvent dispersion & solute cavitation) depending on the surface area (SA) [65].

For each MD simulation, we selected 2000 snapshots and, upon removal of the coordinates of water molecules, we computed the DFTB3-PBSA energy of the solute atoms as

$$G_{DFTB3/PBSA} = E_{DFTB3} + \Delta_{solv}G^{PB}_{elec} + \Delta_{solv}G^{SA}_{non-polar} \qquad (1)$$

The DFTB3 energies were computed using the sander program and complemented with dispersion and hydrogen-bonding corrections [66] evaluated with the Cuby4 framework [67]. The non-linear PB equation was solved on a cubic lattice by using an iterative finite-difference method and taking modified Bondi atomic radii assigned by the tLeap program and the Mulliken DFTB3 atomic charges of the solute atoms. We chose a grid spacing of 0.33 Å, null ionic strength and building the dielectric boundary as the contact surface between the radii of the solute and the radius (1.4 Å) of a water probe molecule. The internal and external dielectric constant values $\varepsilon_{int} = 1$ and $\varepsilon_{out} = 80$, respectively, were used in the PB calculations. The PBSA program in the AMBER suite was used to calculate both the electrostatic PB energies and the non-polar solvation terms.

The statistical uncertainty of the average values $\bar{G}_{DFTB3/PBSA}$ was estimated by computing the block-averaged standard errors of the mean (be). To this end, the MD snapshots were divided into segments ("blocks") with a block size M that corresponds to a quarter of the total number of frames.

2.7. Absolute entropy calculations

Since host-guest binding processes normally involve large entropy changes, we carried out absolute entropy calculations in order to complement the DFTB3/PBSA energies and estimate binding free energies. To this end, we follow the approximation introduced by Karplus et al. that describes the potential energy surface of flexible molecules populating multiple conformational states as a collection of disjoint harmonic wells [68,69]. In this way, the absolute entropy S can be estimated as:

$$S = \bar{S}_{RRHO} + S_{conform} \qquad (2)$$

where $\bar{S}_{RRHO}$ is the average entropy over the set of energy wells associated to the translational + rotational + vibrational degrees of freedom. Each S_{RRHO} value is obtained by computing the MM Hessian matrix of the corresponding energy-minimized structure and applying statistical formulas derived within the rigid rotor and harmonic oscillator (RRHO) approximations. On the other hand, $S_{conform}$ is the conformational contribution that arises from the discrete probability distribution associated to the population of the different minima. The vibrational term in $\bar{S}_{RRHO}$ collects the entropic contributions of small amplitude motions, while $S_{conform}$ accounts for the entropy arising from large amplitude internal motions related to conformational transitions.

The RRHO entropy calculations were performed on the MD snapshots extracted along the MD trajectories for the energetic analysis. Prior to the normal mode calculations, the geometries of the systems were minimized until the RMSD of the elements in the gradient vector is less than 10^{-6} kcal mol^{-1} Å^{-1}. To avoid extensive changes in the internal geometry [70], the systems were prepared by extracting, from the corresponding MD snapshots, the coordinates of the solute atoms and those of a buffer layer of waters with a ~ 6 Å thickness around the solute atoms. During the energy minimizations, the water molecules were fixed. Subsequently, the geometrical calculation of the Hessian matrix and the normal mode calculations were restricted to the active region comprising the solute atoms. The geometry minimizations were driven by the Truncated-Newton Conjugate Gradient method implemented in the sander program and the normal mode calculations were performed using a locally modified version of the nmode program. The quasi-RRHO approximation [71] was applied to reduce the overestimation of vibrational entropies associated to small-frequency normal modes. A 1.0 M standard state concentration was assumed for the translational entropy.

Conformational entropies ($S_{conform}$) were calculated using the CENCALC program [72]. This program selects a set of rotatable dihedral angles using both trajectory coordinates and topology information. It discretizes the time evolution of the selected dihedral angles by evaluating their continuous probability density functions (PDFs) represented by a von Mises kernel density estimator, which depends on a concentration parameter κ (a $\kappa = 0.35$ value was chosen here). By finding the maxima and minima of the PDF, the time series containing the values of the corresponding dihedral angle during the MD simulation is transformed into an array of integer numbers labelling the accessible conformational states, which in turn is processed to estimate the rate of conformational change along the MD trajectory.

CENCALC calculates first unidimensional probability mass functions and readily computes the marginal (first-order) conformational entropy of each dihedral. Correlation effects into $S_{conform}$ were estimated using an expansion technique, termed multibody local approximation (MLA), which can be formally expressed as a sum of conditional entropies [73]. Prior to the MLA calculations, the internal rotations were categorized as having "fast", "medium" or "slow" conformational rates following the prescriptions that have been previously described for CDs systems [4]. In this way, the MLA entropy calculations included correlation effects between dihedral angles belonging to the same group, leading thus to a significant reduction in the number of conformational degrees of freedom that have to be considered. In addition, the bias of the MLA entropy due to finite sampling was minimized by shuffling the elements of the arrays of integer numbers labelling the conformational states.

3. Results and discussion

3.1. Molecular dynamics simulations of β-CD-C$_n$

The conformational space sampled by the amphiphilic CDs was first characterized in terms of the ϕ and Ψ dihedral angles defined for the rotation around the flexible glycosidic bonds between consecutive sugar rings. Fig. 1 shows the contour maps obtained for the distribution of these ϕ (H1$_{(i)}$-C1$_{(i)}$-O4$_{(i-1)}$–C4$_{(i-1)}$) and Ψ (C1$_{(i)}$-O4$_{(i-1)}$-C4$_{(i-1)}$-H4$_{(i-1)}$) values in the β-CD and β-CD-C$_n$ systems. In these plots, the symmetrical conformation with all the glucose rings aligned almost parallel with respect to the CD ring axis corresponds to ϕ and Ψ values around zero. This (0°, 0°) region is not highly populated in the contour maps and, accordingly, the perfect toroidal conformation hardly arises during the MD simulations in aqueous solution. Two or three peaks were observed in the (ϕ, Ψ) contour maps for the different β-CD-C$_n$ molecules, what confirms the intrinsic flexibility of the β-CD ring. The most populated conformation, which appears at ϕ values around −50° in β-CD, is shifted slightly upwards in the three β-CD-C$_n$ variants. The additional secondary peaks mainly result from the multimodal character of the Ψ distribution (see Fig. S1). Particularly, the peak located at Ψ values around 150° in β-CD and β-CD-C$_4$ results from the tilting inwards of some of the sugar rings. The presence of the alkyl side chains in the amphiphilic derivatives somehow impedes such inward tilting of the glucoses as confirmed by the progressive decrease in the population of Ψ values around 150° (see below). In contrast, a new peak located at Ψ values around 50° becomes populated in the β-CD-C$_n$ systems.

The ability to form inclusion complexes with guest molecules and their stability clearly depend on the size of the central cavity of the CD host. Fig. 1 also collects a histogram representation of the radius of accessibility computed for the different β-CD-C$_n$ cavities as explained in Methods. As expected, the presence of the alkyl side chains in β-CD-C$_n$ reduces the accessibility to the central cavity of the β-CD ring. The largest reduction occurs for β-CD-C$_{10}$ that presents a very small average radius of accessibility (0.5 Å), derived from a high percentage of conformations (close to 35%) with a completely occluded cavity. In addition, the distribution of r_{acc} values points to β-CD-C$_{10}$ as the most rigid system. β-CD-C$_4$ and β-CD-C$_{14}$ present better accessibilities to the central cavity, but they are still significantly reduced when compared to the one computed for the unsubstituted β-CD ring.

To further characterize the conformations sampled by the amphiphilic CDs in solution, Fig. 1 displays the last structure from each simulation, while Fig. S2 presents the cluster representatives of the most populated clusters obtained by considering the RMSD values of the heavy atoms in the CD ring. Inspection of Fig. S2 shows the prevalence of distorted rings (*i.e.*, that deviate from a perfect toroidal arrangement) in all the β-CD-C$_n$ simulations. In addition, the comparison of the abundances of the different clusters with those previously reported for the unsubstituted β-CD (see Table S2) [4] confirms the reduction in the flexibility of the β-CD ring associated to the presence of the alkyl side chains.

The stiffening of the CD ring is particularly remarkable for β-CD-C$_{10}$, where most of the MD snapshots (75%) are included in the first cluster. In the corresponding cluster representative, the C$_{10}$ alkyl side chain bound to the third glucopyranose unit (*i.e.* MD numbering) bends to enter the CD cavity through the wide opening with the terminal methylene group exiting through the narrow rim. In the rest of the β-CD-C$_{10}$ clusters shown in Fig. S2 and in the last structure included in Fig. 1, only the central methylene groups of chain 3 reside in the hydrophobic cavity. The time evolution and
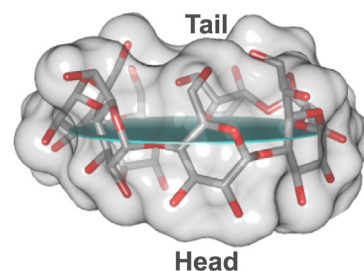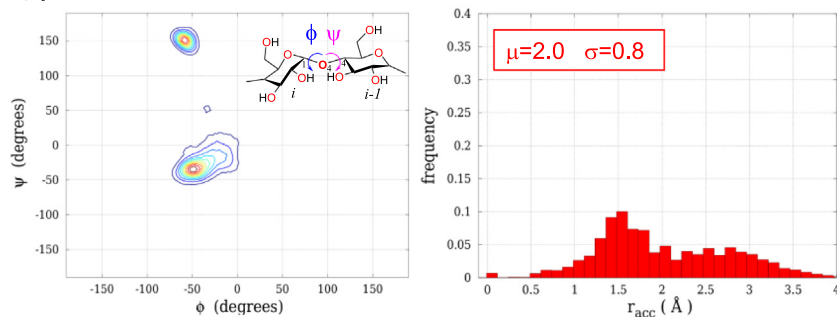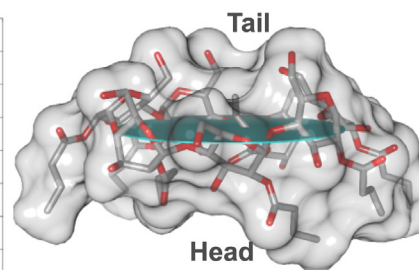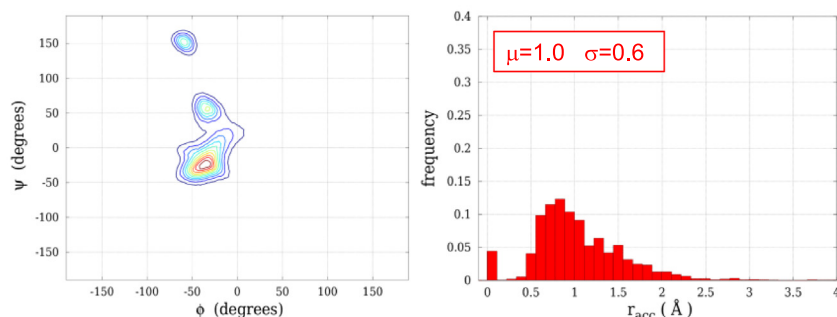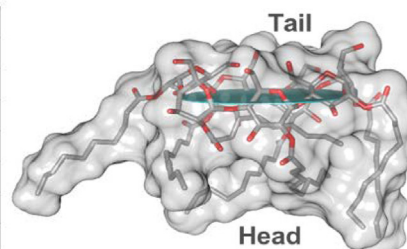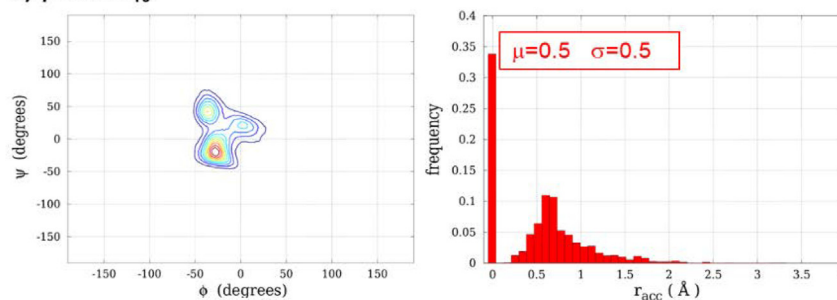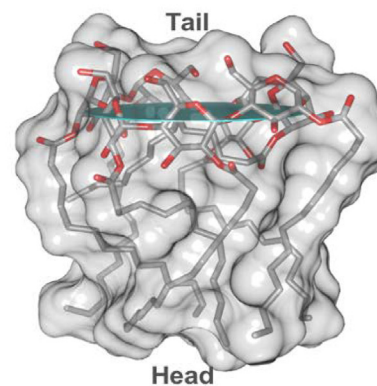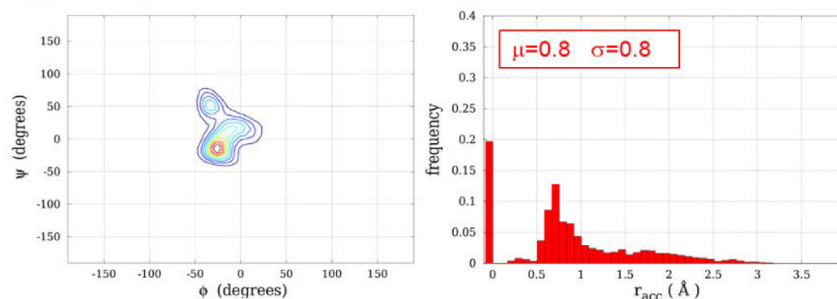
Fig. 1. Contour maps for the Φ_i (H1$_{(i)}$-C1$_{(i)}$-O4$_{(i-1)}$-C4$_{(i-1)}$) and Ψ_i (C1$_{(i)}$-O4$_{(i-1)}$-C4$_{(i-1)}$-H4$_{(i-1)}$) dihedral angles derived from the MD simulations of the different β-CD-C$_n$ variants. Histogram representation of the radius of accesibility (r_{acc}) to the center of mass of the cyclodextrin ring. The average value (μ) and the standard deviation (σ) of r_{acc} are also provided for each system. Last structure from the different simulations, with CD represented by a stick model (without Hs) enclosed by its molecular surface (transparent grey). Water molecules are omitted for clarity. The disc in green-blue correspond to the plane defined by the glycosidic O4 atoms.

the average value of the molecular surface computed for the 1–7 alkyl side chains (see Fig. S3) confirms that chain 3 presents a significantly reduced average molecular surface (52 Å^2) with a steady time evolution during most of the β-CD-C$_{10}$ simulation. Thus, once a chain is properly bound within the central cavity of the β-CD-C$_{10}$ ring, it is not easily displaced by the other alkyl fragments. This

placement of an alkyl side chain within the hydrophobic cavity impedes the tilting inwards of the glucose rings and reduces the Ψ values around 150°.

The other two amphiphilic molecules, β-CD-C$_4$ and β-CD-C$_{14}$, present a similar tendency to place their alkyl side chains within the cavity, but with some particularities associated to their differ-

ent lengths. Most of the snapshots in the β-CD-C$_4$ simulation present one side-chain entering the cavity, but there is also a significant percentage of frames with an empty cavity and opposed sugar rings tilted inwards (see clusters 3 and 4 with populations of 7.6% and 5.1% in Fig. S2). Moreover, the identity of the included alkyl moiety changes along the β-CD-C$_4$ simulation (see Fig. S3). For β-CD-C$_{14}$, the long alkyl side chain allows chain 5 to cross the cavity during most of the 5 µs of simulation time. Nonetheless, the presence of the alkyl groups within the cavity is compatible with some degree of flexibility in the backbone of the CD ring, as confirmed by the presence of two major clusters with a similar population (40% and 31%). We also observed that chain 5 exits the cavity during the last part of the simulation (see the time plots in Fig. S3), while chain 2 is placed in the vicinity of the cavity without crossing it (see Fig. 1 and cluster 4 in Fig. S2c).

To analyze the effect of the alkyl side chains on the solvation of the β-CD ring, we characterized the solute–solvent H-bond contacts involving the primary (O6) and secondary (O2 and O3) alcohol groups (see Table S3). We found that the alkyl side chains do not perturb the hydration of the primary alcohols located at narrow rim, whereas the O3 secondary alcohols located at the wide rim tend to give less interactions with water molecules as the length of the alkyl side chains bound to O2 increases. For instance, the average number of water molecules involved in O3···H@Wat contacts shifts from 4.9 for β-CD to 4.4, 3.5, and 3.1 for the β-CD-C$_n$ derivatives with C$_4$, C$_{10}$, and C$_{14}$ side chains, respectively.

3.2. β-CD/diazepam and β-CD-C$_n$/diazepam inclusion complexes

Various relative orientations between β-CD and Dzp were considered for the initial inclusion complexes that differ in the identity of the Dzp fragment included within the β-CD ring and in the entrance door to the β-CD cavity. Thus, the chlorobenzene (ClPhe) or the phenyl ring (Phe) bound to the central 1,4-diazepin-2-one moiety in Dzp (see scheme 2) were alternatively placed within the β-CD ring. In addition, the inclusion of the drug can proceed through the head (H: the wide rim with the secondary alcohols) or the tail (T: the narrow rim). As a result, four *initial* host–guest arrangements denoted as β-CD/Dzp$_{(Phe-H)}$, β-CD/Dzp$_{(Phe-T)}$, β-CD/Dzp$_{(ClPhe-H)}$, and β-CD/Dzp$_{(ClPhe-T)}$ were subject to extensive simulation in order to analyze their structural stability and predict the preferred binding mode (see Scheme 3 and Fig. S4).

During the four β-CD/Dzp simulations, the guest remains essentially bound within the cavity of the host as indicated by the time evolution of the distance between the centers of mass of the β-CD and Dzp molecules, and the three Euler angles describing the orientation of Dzp with respect to the β-CD ring (see Fig. S5). The shortest average distance (2.0 Å) is computed for the β-CD/Dzp$_{(Phe-H)}$ simulation, and the time evolution of the Euler angles confirms that Dzp maintains its initial position within the β-CD ring during the whole trajectory (see Fig. 2a). However, along the other three simulations (β-CD/Dzp$_{(Phe-T)}$, β-CD/Dzp$_{(ClPhe-H)}$, and β-CD/Dzp$_{(ClPhe-T)}$), the initial host–guest arrangement evolved as indicated by the significant changes of the β-CD···Dzp distance/Euler angles. To provide further details of the resulting β-CD/Dzp structures, Fig. S6 displays snapshots extracted from the MD simulations at regular time intervals and the corresponding θ angle formed between the planes defined by the glycosidic O4 atoms in β-CD and the Phe ring in Dzp. The eight structures collected from the β-CD/Dzp$_{(Phe-H)}$ trajectory (Fig. S6a) consistently display the guest molecule bound through the CD head with the Phe group well inserted within the β-CD cavity and oriented almost perpendicular to the β-CD ring (θ ~ 90°). In contrast, Dzp changed its initial position at the tail during the second half of the β-CD/Dzp$_{(Phe-T)}$ simulation (see the last three frames in Fig. S6b) and adopted a similar configuration to that observed in β-CD/Dzp$_{(Phe-H)}$. The other

two binding modes that initially placed the ClPhe fragment of Dzp within the β-CD cavity were dynamically unstable. The guest crossed the β-CD cavity at the very beginning of the β-CD/Dzp$_{(ClPhe-H)}$ and β-CD/Dzp$_{(ClPhe-T)}$ simulations, to start sampling states that formally corresponds to the initial β-CD/Dzp$_{(Phe-T)}$ and β-CD/Dzp$_{(Phe-H)}$ configurations, respectively (see Fig. S6). The Dzp guest keeps its Phe ring inserted through the tail of the β-CD ring during the whole β-CD/Dzp$_{(ClPhe-H)}$ simulation, while it rotates at the head of the host molecule placing either the Phe or the diazepine ring within the hydrophobic cavity in the β-CD/Dzp$_{(ClPhe-T)}$ trajectory (see Figs. S5 and S6). Therefore, the β-CD/Dzp simulations safely discard the binding of the chlorophenyl moiety of Dzp within the β-CD cavity.

Taking into account the results obtained from the four β-CD/Dzp simulations, only the complexes with the Phe group inserted at the head or at the tail of the β-CD-C$_n$ cavity were prepared for the simulations of the amphiphilic derivatives. The simulations were termed as β-CD-C$_n$/Dzp$_{(H)}$ and β-CD-C$_n$/Dzp$_{(T)}$, respectively. Fig. 2 presents the time evolution of the distance between the center of mass of the β-CD-C$_n$ ring and the Dzp guest for selected simulations, while the complete set of β-CD-C$_n$/Dzp distances and the dial plots of Euler angles are included in Fig. S7. In addition, Figs. 2 and S8 display representative structures of the solute molecules extracted from the different simulations.

According to our results, the presence of the alkyl side chains significantly destabilizes the inclusion complexes formed by the β-CD-C$_n$ hosts with Dzp. For example, the average distance between the center of mass of the β-CD ring and the guest increases from 2 to 3 Å in the β-CD/Dzp trajectories to values of 3.6 Å and higher for the amphiphilic derivatives (see Figs. 2 and S7). In addition, the Euler angles show frequent shifts that indicate the tumbling of the guest along the β-CD-C$_n$/Dzp simulations (see Fig. S7). The inclusion of Dzp at the tail of the β-CD-C$_n$ ring is not favorable in any case. Only in the β-CD-C$_4$/Dzp$_{(T)}$ simulation, the initial binding mode remained stable during the first 1.3 µs. Then the guest unbinds and moves to the head of the β-CD-C$_4$ ring, where it oscillates between forming real inclusion complexes (*i.e.* with the Phe group inserted in the hydrophobic cavity) and those where Dzp interacts with the alkyl side chains at the head entrance (see θ values in Fig. S8b). Increasing the length of the C$_n$ chain results in a faster expulsion of Dzp from the tail of the amphiphilic host, the guest molecule being replaced by one alkyl side chain (see the time plots in Figs. S7d, S7f, S9d and S9f). Moreover, the large and flexible C$_{10}$ and C$_{14}$ alkyl side chains impede the diffusion of the expelled Dzp and its binding at the head of the β-CD-C$_n$ ring during the 5 µs of the β-CD-C$_{10}$/Dzp$_{(T)}$ and β-CD-C$_{14}$/Dzp$_{(T)}$ simulations. Along these trajectories, the guest only interacts with the alkyl side chains forming side complexes (*i.e.*, outside the β-CD hydrophobic cavity; see Fig. S8). On the other hand, the inclusion complexes in which Dzp is initially bound through the head of the β-CD-C$_n$ host seem to be structurally more stable. The Phe group of the guest remains roughly included within the CD ring during the β-CD-C$_{14}$/Dzp$_{(H)}$ simulation, while it fluctuates between an included and a partially excluded position in the β-CD-C$_4$/Dzp$_{(H)}$ trajectory. At the end of the β-CD-C$_{10}$/Dzp$_{(H)}$ simulation, the Dzp molecule is displaced from the CD hydrophobic cavity by an alkyl side chain (see chain 5 in Fig. S9c) and it remains partially entangled within the rest of the chains (see Figs. S7c and S8c). This and the rest of MD results derived from the β-CD-C$_n$/Dzp simulations strongly suggest that the inclusion complexes would be energetically much less stable than those of the parent β-CD.

We also assessed the impact of the Dzp molecule on the solute-solvent contacts formed by β-CD and β-CD-C$_n$. With respect to the unbound β-CD state, Dzp binding slightly increases the solvation of the primary alcohol groups located at the tail and simultaneously decreases solvent interactions with the secondary alcohols at the
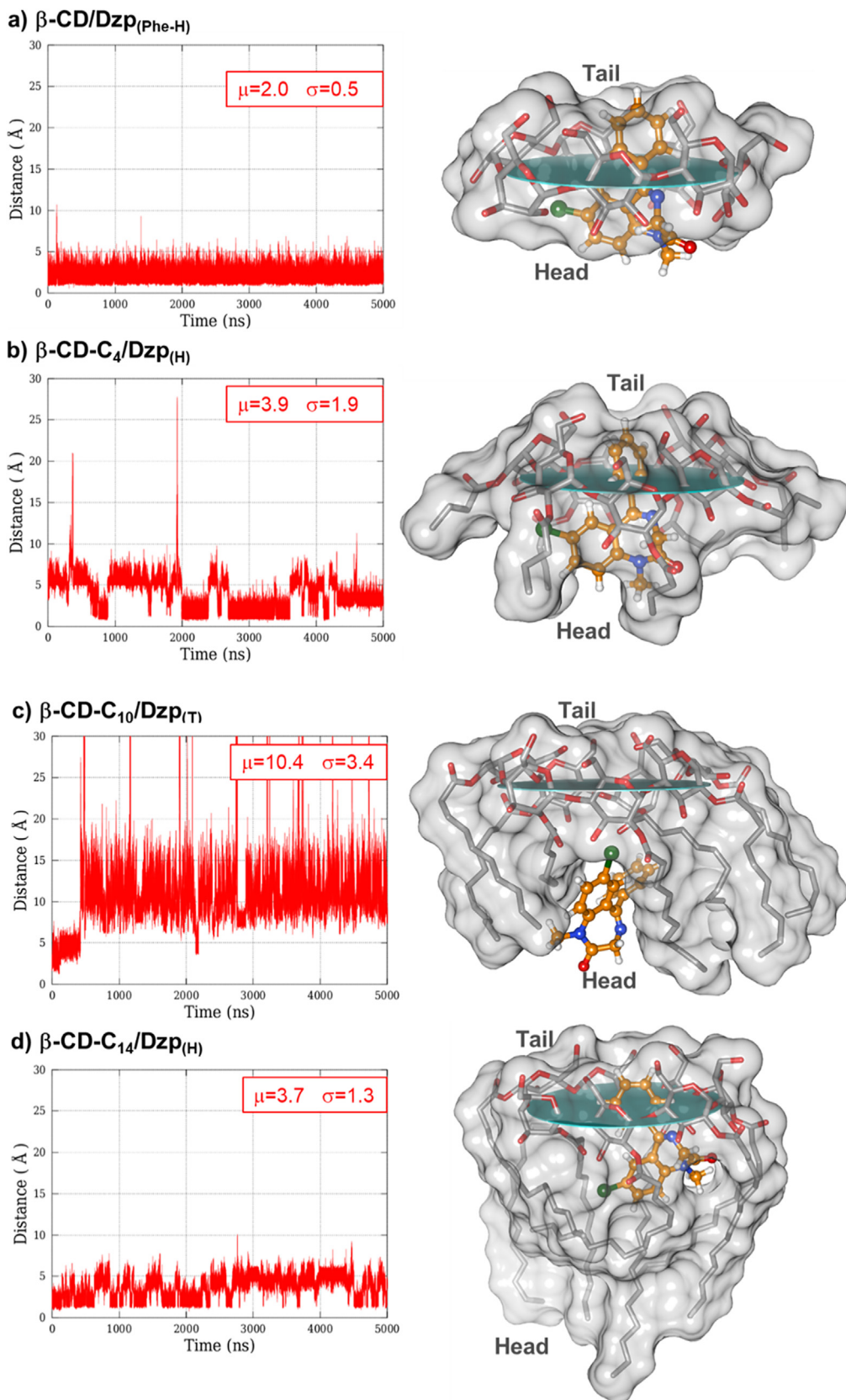
Fig. 2. Time evolution of the distance (Å) between the center of mass of the β-CD ring (C1, C4, and O4 atoms), and the center of mass of the diazepam guest. Average value (μ) and standard deviation (σ) are also provided. Last structure from selected β-CD/Dzp and β-CD-C$_n$/Dzp simulations, with CD represented by a stick model (without Hs) enclosed by its molecular surface (transparent grey), and the guest Dzp in ball-and-stick with carbon atoms in orange (O in red, N in blue, Cl in green, and H in white). The disc in green-blue correspond to the plane defined by the glycosidic O4 atoms. Water molecules are omitted for clarity.

head of the host molecule (see Tables S3 and S4). For instance, the average number of water molecules interacting with the β-CD@O6H groups increases from 5.4 to 5.8–5.9 in the presence of the Dzp guest, while the water molecules H-bonded to β-CD@O2H/O3H decreases from 6.3/5.5 to 5.2–5.5/3.0–3.6 in the different β-CD/Dzp simulations. This trend is also observed for β-CD-C$_4$. In contrast, the presence of Dzp has an almost negligible influence on the solvation of the different alcohol groups in the β-CD-C$_{10}$ and β-CD-C$_{14}$ hosts.

3.3. β-CD/Dzp and β-CD-C$_n$/Dzp binding energies

The binding free energy components estimated for the β-CD/Dzp complexes are collected in Table 1. The $\Delta G_{DFTB3/PBSA}$ and $-T\Delta S_{RRHO}$ values result from the difference of the average $G_{DFTB3/PBSA}$ and S_{RRHO} descriptors derived from three independent simulations (the isolated β-CD and Dzp molecules and the β-CD/Dzp complex). Similarly, the T-weighed conformational entropy change, $-T\Delta S_{conform}$, is obtained by subtracting the limiting values of $S_{conform}$ after 5.0 μs in the three independent MD trajectories. To help interpret the energetic results, Table 1 gives also the abundances of the inclusion binding modes observed during the MD simulations. Such values correspond to the population of cluster representatives that show different host–guest orientations as obtained from clustering calculations considering a 1.5 Å cutoff in the RMSD value of atoms C1, C4, and O4 in the host and the C, N, and O atoms in Dzp.

For the unsubstituted β-CD, the global ΔG scorings are very similar, ranging between −5.3 and −6.2 kcal/mol, with statistical uncertainties below 0.8 kcal/mol. The relatively large magnitude of these ΔG values is consistent with the structural stability and preferred binding modes observed in the simulations. The lowest one corresponds to the β-CD/Dzp$_{(Phe-H)}$ trajectory, which exhibits a single binding mode (100% abundance) characterized by the placement of the guest at the head entrance of the β-CD ring with its Phe group well included within the hydrophobic cavity (see Fig. 2). The structurally similar β-CD/Dzp$_{(ClPhe-T)}$ simulation turns out to be slightly less stable (ΔG = -5.3), probably due to the exchange between the Phe and diazepine rings within the β-CD cavity. Considering the binding through the β-CD tail, which is dominant in β-CD/Dzp$_{(ClPhe-H)}$ and also present in the β-CD/Dzp$_{(Phe-T)}$ simulation, the values in Table 1 suggest that this binding mode would be slightly less stable (∼0.2–0.9 kcal/mol) than that involving the Phe binding at the head entrance.

Experimentally, the standard ΔG value reported for the β-CD/Dzp complex amounts to −5.7 kcal/mol, as obtained by means of non-linear fitting to solubility data of Dzp in aqueous solution at varying concentrations of β-CD [74]. The most favorable ΔG value

in Table 1 (-6.2 kcal/mol) is quite close to the experimental value. Taking into account that end-point free energy calculations usually overestimate binding free energies for protein–ligand or host–guest complexes owing to their intrinsic limitations (*e.g.* unbalanced enthalpy/entropy estimations) [75], the good agreement between our calculations and the experimental value may partially result from cancelation of errors. In any case, the free energy *rankings* expressed in terms of relative $\Delta\Delta G$ values usually have a significant predictive capacity [76] and, therefore, we focus on the $\Delta\Delta G$ trends in the unsubstituted β-CD and in the esterified derivatives. In this respect, the presence of the alkyl side chains in the amphiphilic β-CD-C$_n$ derivatives systematically reduces the ΔG scorings by ∼6 or ∼11 kcal/mol (see Table 1). Such energetic destabilization is in consonance with the loose/variable intermolecular contacts and frequent host-guest separation events observed in the β-CD-C$_n$/Dzp MD trajectories.

The ΔG values in Table 1 may also illustrate some interesting aspects of the host-guest interactions and the role of the alkyl chains in the β-CD-C$_n$/Dzp complexes. On one hand, Dzp binding to β-CD-C$_{10}$ is favored by the $S_{conform}$ changes in contrast with the case of the C$_4$ and C$_{14}$ derivatives. This entropic effect is due to the low conformational variability observed for the isolated β-CD-C$_{10}$ molecule, in which one C$_{10}$ alkyl chain fully occupies the β-CD cavity on the μs time scale. The self-inclusion arrangement is perturbed by the presence of the Dzp guest, increasing thus the flexibility of the β-CD-C$_{10}$ moiety. On the other hand, it is clear that the β-CD-C$_n$ monomers have little affinity for prototypical guests like Dzp, the actual ΔG value being clearly positive for β-CD-C$_4$. According to the ΔG estimations, the inclusion complexes would be favored in the presence of large alkyl side chains (1.0 ± 1.2 kcal/mol in β-CD-C$_{14}$/Dzp). However since the Dzp guest did not access spontaneously to the β-CD cavity along the extensive 5.0 μs β-CD-C$_{14}$/Dzp$_{(T)}$ simulation, it turns out that the complex dynamics of the long and flexible C$_n$ moieties may hamper the diffusion of guest molecules within the β-CD ring, exerting thus a certain kinetic control of the binding process.

To better understand the negative impact of the β-CD *trans*-esterification on the Dzp binding ability, we estimated the DFTB3 and PBSA deformation energies of the β-CD-C$_n$ molecules upon the complexation process (see the $\Delta_{def}E_{DFTB3}$ and $\Delta_{def}G_{PBSA}$ data in Table S5). We found that structural rearrangements in the host molecules penalize the formation of the β-CD-C$_n$/Dzp complexes, resulting in relatively large values of $\Delta_{def}E_{DFTB3}$ ranging from +4 to +25 kcal/mol depending on the trajectory (the equivalent $\Delta_{def}G_{PBSA}$ values fluctuate between −3 and 2 kcal/mol). In contrast, the rearrangement of the CD molecule favors Dzp binding to the native β-CD as indicated by $\Delta_{def}E_{DFTB3}$ values about −17 kcal/mol,

Table 1
Average values (in kcal/mol) of the gas-phase plus solvation ($\Delta G_{DFTB3/PBSA}$) and entropy ($-T\cdot\Delta S_{RRHO}$ and $-T\cdot\Delta S_{conform}$) contributions to the binding free energies (ΔG) computed for the different β-CD/Dzp and β-CD-C$_n$/Dzp simulations. Numbers in parentheses correspond to the block-averaged standard errors of the mean. Abundances (%) of the inclusion binding modes as derived from clustering analysis are also given.

MD trajectory [1]	% Inclusion binding mode	$\Delta G_{DFTB3/PBSA}$	$-T\cdot\Delta S_{RRHO}$	$-T\cdot\Delta S_{conform}$	ΔG
β-CD/Dzp$_{(Phe-H)}$	Phe(Dzp) at Head-CD (100%)	−24.0 (0.3)	14.9 (0.1)	2.9	−6.2 (0.3)
β-CD/Dzp$_{(Phe-T)}$	Phe(Dzp) at Tail-CD (64%)	−22.0 (0.6)	15.0 (0.2)	1.7	−5.3 (0.6)
	Phe(Dzp) at Head-CD (29%)				
β-CD/Dzp$_{(ClPhe-H)}$	Phe(Dzp) at Tail-CD (100%)	−22.4 (0.4)	14.7 (0.3)	1.7	−6.0 (0.5)
β-CD/Dzp$_{(ClPhe-T)}$	Phe(Dzp) at Head-CD (74%)	−23.0 (0.8)	14.5 (0.1)	3.2	−5.3 (0.8)
	Diazepine(Dzp) at Head-CD (24%)				
β-CD-C$_4$/Dzp$_{(H)}$	Dzp at Head-CD (52%)	−17.1 (2.1)	15.6 (0.4)	5.2	3.7 (2.1)
β-CD-C$_4$/Dzp$_{(T)}$	Dzp at Head-CD (39%)	−14.0 (2.7)	15.4 (0.2)	3.5	4.9 (2.7)
	Dzp at Tail-CD (27%)				
β-CD-C$_{10}$/Dzp$_{(H)}$	Dzp at Head-CD (37%)	−10.5 (1.7)	15.2 (0.3)	−3.3	1.4 (1.7)
β-CD-C$_{10}$/Dzp$_{(T)}$	Dzp at Tail-CD (9%)	−8.4 (2.4)	15.4 (0.4)	−5.7	1.3 (2.4)
β-CD-C$_{14}$/Dzp$_{(H)}$	Dzp at Head-CD (99%)	−19.3 (0.9)	15.3 (0.8)	5.0	1.0 (1.2)
β-CD-C$_{14}$/Dzp$_{(T)}$	Dzp at Tail-CD (1%)	−13.0 (0.8)	15.6 (0.6)	2.3	4.9 (1.0)

[1] MD labelling denotes the initial host–guest arrangement. See text and Fig. S4 for details.

which are not compensated by $\Delta_{def}G_{PBSA}$ values about +9 kcal/mol. We found that this energetic preference can be explained in terms of the rigidifying effect played by the small Dzp molecule on the β-CD macrocycle that, in turn, favors the formation of intramolecular H-bonds among the secondary hydroxyl groups of consecutive residues. For example, the abundance of R_i@O3H···O2@R_{i+1} contacts between consecutive sugar units augments from 8–10% (β-**CD**) to 32–39% (β-**CD/Dzp(Phe-H)**). However, the flexibility of the CD macrocycle in the β-CD-C_n molecules is more largely influenced by the C_n alkyl chains, whose intramolecular packaging is perturbed by the presence of Dzp, explaining thus the $\Delta_{def}E_{DFTB3}$ penalty.

3.4. MD simulations of the β-CD and β-CD-C_n homodimers

According to the packaging of native CDs in crystal structures [9], the β-CD monomers in the dimer states may adopt a channel-type (*i.e.* parallel rings with the cavities aligned), a layer-type (*i.e.* parallel rings with the cavities not aligned), a cage-type (*i.e.* perpendicular rings), or an intermediate V-type geometry (see Scheme 4). We considered two limiting channel-arrangements in order to build the initial geometry of the dimers and to facilitate the sampling of intermediate arrangements during the 5 μs-long MD simulations. Thus, in the head-to-head dimer (HH), the secondary rims or wide edges of the CD cones (see Scheme 4) are initially facing each other, while the primary rims or narrow edges are face-to-face in the initial tail-to-tail dimer (TT). These resulted in the β-CD/β-CD(HH), β-CD/β-CD(TT), β-CD-C_4/β-CD-C_4(HH), β-CD-C_4/β-CD-C_4(TT), β-CD-C_{10}/β-CD-C_{10}(HH), β-CD-C_{10}/β-CD-C_{10}(TT), β-CD-C_{14}/β-CD-C_{14}(HH), and β-CD-C_{14}/β-CD-C_{14}(TT) initial dimers. Fig. 3 shows the time evolution of the distance between the center of mass of the β-CD rings in selected simulations and the corresponding histogram representation of the θ angle between the planes defined by the glycosidic O4 atoms in each CD ring. Further MD results like the time evolution of the Euler angles for the relative orientation of both CD rings and the

contact surface area between the two CD monomers are presented in the SI for all the β-CD/β-CD and β-CD-C_n/β-CD-C_n simulations (Figs. S10-S15).

According to the evolution of the CD···CD distances (see Fig. S10) and the contact area values (see Fig. S11), numerous transitions between the dimer and the separated monomers occur during the β-CD/β-CD(HH), and β-CD/β-CD(TT) simulations. Although some dimer ↔ monomer transitions are also observed in the β-CD-C_4/β-CD-C_4(TT) trajectory (see Fig. 3), the presence of the alkyl side chains in the β-CD-C_n molecules tends to favor the dimer state, which is in general perfectly stable in the case of the β-CD-C_{10} and β-CD-C_{14} systems. The average CD···CD rings distance in the dimers increases with the length of the alkyl side chains, from 7 Å as measured in the steady portions of the β-CD/β-CD simulations to 10, 15, and 22 Å obtained for the β-CD-C_4, β-CD-C_{10}, and β-CD-C_{14} dimers, respectively, as a consequence of the involvement of the alkyl side chains in β-CD-C_n in the dimer binding. As expected, the magnitude of the contact area between the two monomers augments significantly with the size of the monomers (see Fig. S11). Moreover, it turns out that the dimers become much more compact with the lengthening of the alkyl side chains given that the percentage ratio between the contact area and the total monomer areas increases from ∼25% in the β-CD/β-CD simulations to ∼40% in β-CD-C_{14}/β-CD-C_{14}, what suggest that an important hydrophobic effect may be at work for the larger dimers.

The conformation of the macrocyclic rings is moderately affected by the dimerization process as shown by the comparison of the ϕ/Ψ contour maps obtained from the simulations of the dimers (Fig. S12) and those of the monomers (Fig. 1). In the β-CD/β-CD dimer, it seems that one of the monomers is more distorted than the other one (CD2 in the β-CD/β-CD(HH) simulation and CD1 in the β-CD/β-CD(TT) trajectory). For the β-CD-C_4 dimers, both monomers are similarly distorted in the β-CD-C_4/β-CD-C_4(HH) trajectory and they remain essentially unchanged in the β-CD-C_4/β-CD-C_4(TT) simulation. The β-CD ring moieties seem slightly distorted in the β-CD-C_{10} and β-CD-C_{14} dimers, albeit more accen-
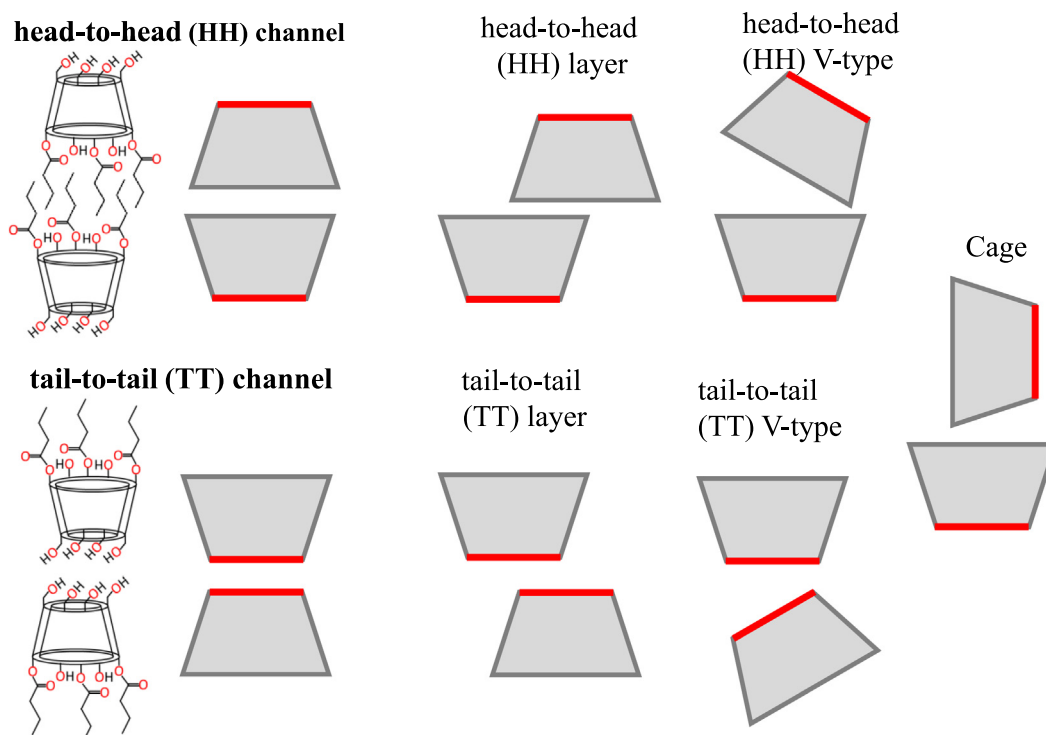
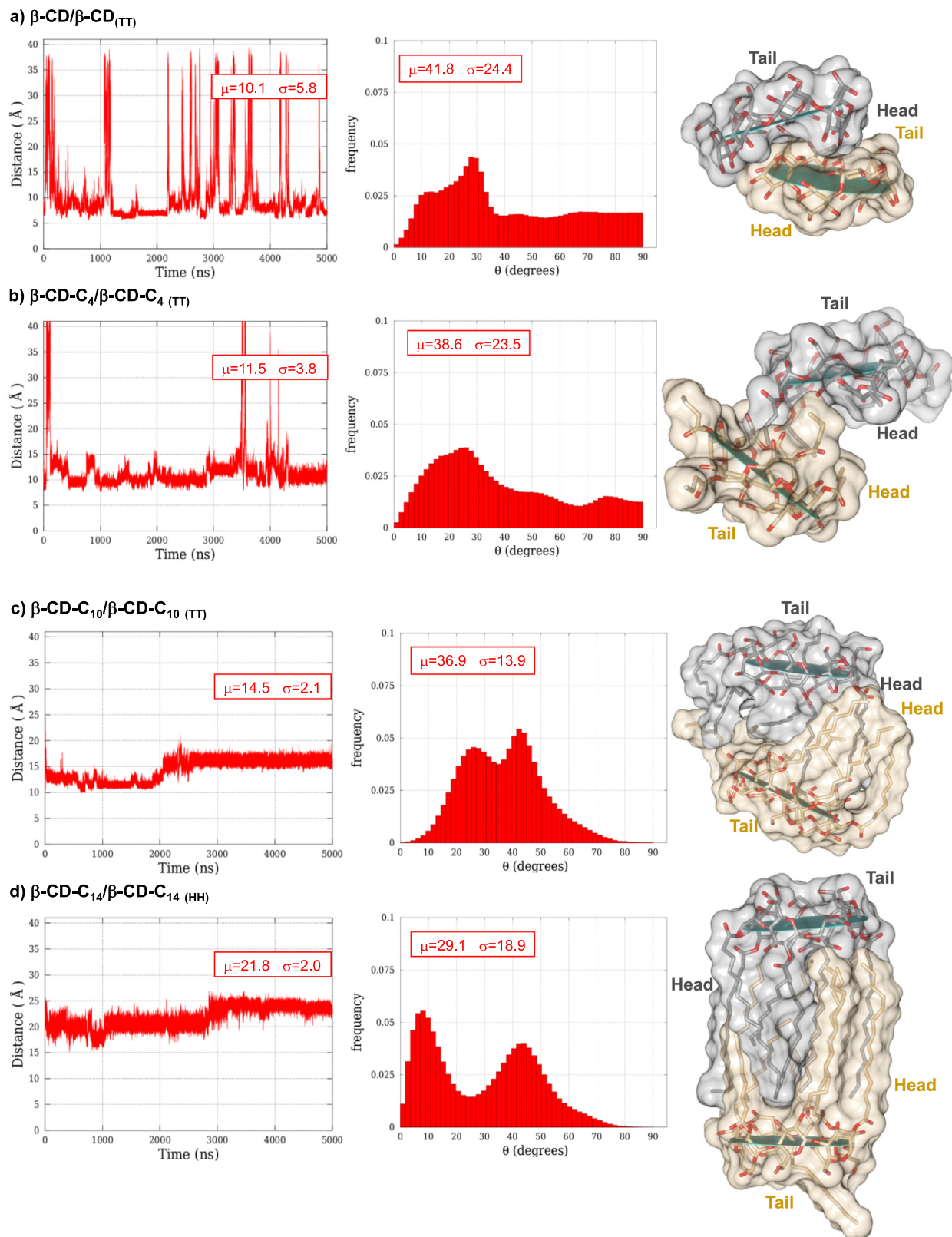**Scheme 4.** Alternative arrangements for the β-CD/β-CD dimers and their amphiphilic derivatives.

Fig. 3. Time evolution of the distance (Å) between the center of mass of the β-CD rings (C1, C4, and O4 atoms) in selected β-CD-C$_n$/β-CD-C$_n$ simulations. Histogram representation for the angle θ (°) between the planes defined by the glycosidic O4 atoms (green-blue discs in the images). Average values (μ) and standard deviations (σ) are also provided. Last structure from simulation with CDs represented by a stick model (without Hs) enclosed by its molecular surface (transparent grey for CD1 and transparent brown for CD2). Water molecules are omitted for clarity.

tuated along the β-CD-C$_{10}$/β-CD-C$_{10(TT)}$ trajectory. As in the case of the isolated monomers, the inward tiltering of the glucose rings is largely impeded in the β-CD-C$_{10}$ and β-CD-C$_{14}$ dimers (as shown by the lack of Ψ peaks around ±150°), signaling thus the inclusion of the large alkyl side chains within the β-CD cavity.

The relative orientation of the CD rings in the dimers is quite flexible and exhibits particular features in each trajectory. Such variability can be glimpsed in the Euler plots in Fig. S10 as well as in Fig. S14, which represents MD snapshots extracted from the different β-CD/β-CD and β-CD-C$_n$/β-CD-C$_n$ simulations at regular intervals, and in Fig. 3, which displays the last structure obtained from the selected simulations. To better characterize the dimer arrangements, the histograms of the θ angle between the two CD rings were also calculated (see Figs. 3 and S13).

In the case of the native β-CD, the initial HH and TT channel-type geometries were lost in favor of the most abundant head-to-tail (HT) V-type arrangement. In most of these HT V-type orientations, a primary –CH$_2$OH alcohol group from one of the monomers is included within the wide rim of the other monomer (see for example the 625 ns snapshot in Fig. S14a). The identity of the included primary alcohol changes during the β-CD/β-CD$_{(HH)}$ and β-CD/β-CD$_{(TT)}$ simulations. V-type geometries with HH and TT orientations also arise during the simulations (see frame at 4375 ns in Fig. S14a and frame 1250 ns in Fig. S14b). In addition, cage-type geometries with both CD rings arranged almost perpendicular (θ > 70°) and presenting one CD molecule slightly included at the head (wide rim) of the other molecule are observed in the β-CD/β-CD simulations (see frames at 1250 ns and 3750 ns in Figs. S14a and S14b, respectively). Such structural variability is also evident in the histogram representation of the θ angle (see Fig. S13) and further confirms that the dimer state of the β-CD is highly flexible. In line with the presence of these multiple arrangements between both β-CD molecules, solvent interactions at the primary and secondary alcohols are reduced in the dimer state compared to that in the monomer (see Tables S3 and S6).

The alkyl side chains bound to the O2 secondary alcohols in the wide rim of the β-CD-C$_n$ molecules select particular configurations for the dimers. In general, the β-CD-C$_n$ dimers populate a variety of HH conformations during the MD simulations, the initial TT arrangements in the β-CD-C$_n$/β-CD-C$_{n(TT)}$ dimers being lost rapidly. Therefore, the interactions among the alkyl side chains located at the head of the two rings drive the aggregation of the amphiphilic β-CD-C$_n$ molecules. Not only the length of the alkyl side chains influences the particular geometry of the dimers, but the initial arrangement, either HH or TT, also determines the population of different phase-space regions. On the one hand, the initial HH orientation, which is favorable for the formation of hydrophobic contacts among the alkyl chains, undergoes moderate fluctuations along the MD trajectories, resulting in HH V-type configurations characterized by relatively narrow distributions of the plane-plane θ angles peaking at small values (∼10–30°). On the other hand, the starting TT structure is not adequate for the hydrophobic packaging of the monomers so that the β-CD-C$_n$ monomers reorient themselves to give a variety of HH structures ranging from small-angle V-type to cage-like or layer-type structures, as observed in the wide and multimodal distributions of the θ angle, with maxima being located at ∼30, ∼50 or ∼80° depending on the system. These general features are again modulated by the length of the C$_n$ chains. For example, the β-CD-C$_{10}$/β-CD-C$_{10(TT)}$ populates two nearby V-type configurations with θ values around 25 and 45°, which remain quite flexible as shown by the instantaneous fluctuations of θ. Perhaps of more interest is the case of the β-CD-C$_{14}$/β-CD-C$_{14(HH)}$ and β-CD-C$_{14}$/β-CD-C$_{14(TT)}$ trajectories, which converge both towards the same nearly-parallel and compact HH alignment having θ values around 10°. These complexes show well-extended and intertwined alkyl-chains, resembling thus an elongated bilayer

structure. Interestingly this elongated dimer structure allows a good solvation of the alcohol groups in the β-CD-C$_{14}$ rings as measured by the average number of water molecules interacting with those groups that is roughly the same in the dimer and in the monomer states (see Tables S3 and S6). In contrast, the C$_{10}$ side chains in β-CD-C$_{10}$/β-CD-C$_{10}$ adopt a twisted conformation so that the global structure is more spherical and the hydration of the secondary alcohol groups (O3) is slightly reduced compared to that in the monomer.

The alkyl side chains in the β-CD-C$_n$ molecules tend to occupy the hydrophobic cavity of the β-CD ring. In the dimer state, this can be achieved by self-inclusion or mutual-inclusion. We observe that the mutual-inclusion of one or two C$_4$ side chains predominates in the β-CD-C$_4$/β-CD-C$_{4(HH)}$ simulation, while the self-inclusion is more abundant in the β-CD-C$_4$/β-CD-C$_{4(TT)}$ trajectory. The identity of the included fragments changes during the simulations, which confirms the flexibility of the β-CD-C$_4$/β-CD-C$_4$ aggregate. Due to the limited length of the C$_4$ side chain, the radius of accessibility to the central cavity in β-CD-C$_4$ is similar in the monomer (1.0 Å) and in the dimer states (0.8–0.9 Å in Fig. S15). Enlarging the alkyl side chains to C$_{10}$ and C$_{14}$ rises the occurrence of self-inclusion in one of the CD molecules of the dimer, which correlates with the reduced accessibility to the corresponding hydrophobic cavity (see r_{acc} values in Fig. S15). The other CD molecule remains accessible through the narrow rim (tail) with average r_{acc} values of 0.8–1.1 Å in β-CD-C$_{10}$/β-CD-C$_{10}$ and of 1.8–1.9 Å in β-CD-C$_{14}$/β-CD-C$_{14}$.

3.5. β-CD and β-CD-C$_n$ dimer binding energies

Table 2, which collects the various energy terms computed for the β-CD and β-CD-C$_n$ dimers, shows that the intermolecular interactions and solvent effects favor dimerization while the global entropy changes penalizes aggregation. With respect to the energetic analysis of CD/Dzp complexes, more sophisticated entropy calculations including explicit solvent contributions would be probably required to obtain more reliable ΔG values for the dimer association. Nevertheless, we believe that the results in Table 2 are qualitatively informative and emphasize a fundamental difference between the β-CD or β-CD-C$_4$ systems and the β-CD-C$_{10}$ or β-CD-C$_{14}$ ones regarding their dimer state, the latter ones having enlarged stability as a consequence of stronger interactions between the monomers and a more favorable hydrophobic packaging among the longer C$_n$ side chains.

The positive ΔG values estimated for the β-CD/β-CD dimers, 8.8 and 15.1 kcal/mol, are well in consonance with the frequent dimer ↔ monomer transitions arising along the 5.0 μs trajectories. Hence, according to the simulations, the β-CD/β-CD dimers would not be thermodynamically stable in (diluted) aqueous solution. In the same conditions, the DFTB3/PBSA and entropy calculations point out that the short-chain ester derivatives β-CD-C$_4$ would no form stable dimers either because their estimated ΔG values are clearly positive, 30.3 and 11.5 kcal/mol. These figures also indicate that the V-type complexes, that are more abundant in the β-CD-C$_4$/β-CD-C$_{4(HH)}$ simulation, would be less stable than the mixture of V- or cage-type structures sampled in the TT trajectory (see Fig. S14). Considering also the statistical uncertainty of the mean values, it turns out that the parent β-CD and its C$_4$-ester derivative have similar ΔG scores in their preferred dimer states.

Basing on Table 2 data, we see that elongation of the C$_n$ alkyl chains results in specific energetic properties for the corresponding dimers. First, the ΔG scorings for the two β-CD-C$_{10}$/β-CD-C$_{10}$ simulations are nearly coincident (0.1 and −0.5 kcal/mol), these values being anyway compatible with a significant affinity for the formation of dimer complexes. However, their similarity results from a certain (and maybe fortuitous) enthalpy/entropy compensation

Table 2
Average values of the surface contact area (in absolute value, Å^2), average number of polar contacts with the percentage of snapshots presenting polar interactions, gas-phase plus solvation ($\Delta G_{DFTB3/PBSA}$) and entropy ($-T \cdot \Delta S_{RRHO}$ and $-T \cdot \Delta S_{conform}$) contributions to the binding free energies (ΔG_{bind}) computed for the different β-CD/β-CD and β-CD-C$_n$/β-CD-C$_n$ simulations. Energetic quantities are in kcal/mol. The percentage of contact area and the block-averaged standard errors of the mean values are indicated in parentheses.

MD trajectory [1]	Surface contact area	Polar contacts	$\Delta G_{DFTB3/PBSA}$	$-T \cdot \Delta S_{RRHO}$	$-T \cdot \Delta S_{conform}$	ΔG_{bind}
β-CD/β-CD$_{(HH)}$	558 (26%)	3.5 (90%)	−0.6 (0.6)	17.3 (0.2)	−1.4	15.1 (0.6)
β-CD/β-CD$_{(TT)}$	508 (23%)	3.1 (87%)	−7.1 (1.5)	17.4 (0.2)	−1.7	8.8 (1.5)
β-CD-C$_4$/β-CD-C$_{4(HH)}$	1083 (32%)	1.3 (84%)	1.7 (2.9)	19.3 (0.1)	9.3	30.3 (2.9)
β-CD-C$_4$/β-CD-C$_{4(TT)}$	812 (25%)	1.9 (88%)	−11.8 (4.6)	18.9 (0.2)	4.4	11.5 (4.6)
β-CD-C$_{10}$/β-CD-C$_{10(HH)}$	1398 (31%)	0.5 (29%)	−16.4 (2.8)	18.1 (0.6)	−1.7	0.1 (2.9)
β-CD-C$_{10}$/β-CD-C$_{10(TT)}$	1827 (38%)	0.9 (40%)	−25.4 (4.7)	18.1 (0.3)	6.8	−0.5 (4.7)
β-CD-C$_{14}$/β-CD-C$_{14(HH)}$	2538 (43%)	0.0 (0%)	−57.0 (4.3)	20.3 (1.6)	20.8	−16.4 (4.6)
β-CD-C$_{14}$/β-CD-C$_{14(TT)}$	2622 (43%)	0.0 (0%)	−54.7 (3.2)	19.7 (1.0)	21.7	−13.0 (3.5)

between the lower entropic penalty of the quite flexible β-CD-C$_{10}$/β-CD-C$_{10(TT)}$ and the larger favorable DFTB3/PBSA energy in the more compact and rigid V-type β-CD-C$_{10}$/β-CD-C$_{10(TT)}$ one. For the larger β-CD-C$_{14}$/β-CD-C$_{14}$ dimers, the differences in the DFTB3/PBSA and entropic terms are small and comparable to their statistical uncertainties, what seems in consonance with the fact that the initially distinct β-CD-C$_{14}$ trajectories converge to sample very similar bilayer-type structures. Furthermore, the computed ΔG values (-16.4 and −13.0 kcal/mol) are well below 0.0, pointing out that β-CD-C$_{14}$ possesses a strong preference for the dimerization (and eventually aggregation) process.

3.6. Comparison with experiment

Compared to the unsubstituted β-CD molecule, the monomeric state of the β-CD-C$_n$ derivatives with C$_4$, C$_{10}$, and C$_{14}$ alkyl side chains ester-bound at the wide rim (C2 atoms) exhibits structural particularities in aqueous solution. For example, the inward tilting of the glucopyranose units characterizing the dynamic of the β-CD ring in solution [4], is reduced in the presence of the alkyl groups, the accessibility to the hydrophobic cavity diminishes, and the CD ring becomes more rigid. All these effects are significantly tuned by the length of the grafted C$_n$ fragment. In the β-CD-C$_4$ molecule, several alkyl side chains alternate within the cavity and the inward tilting of the glucose rings is not completely abolished. In contrast, the MD simulations of the β-CD-C$_{10}$ and β-CD-C$_{14}$ molecules show that the self-inclusion of one of the C$_n$ moieties is quite persistent. Compared to C$_4$, the C$_{10}$ and C$_{14}$ fragments are long enough to allow the included side chain to cross the β-CD cavity. We also observe that the larger C$_{14}$ side chain is also compatible with a more flexible β-CD ring.

The self-inclusion of the alkyl-side chains along the monomeric β-CD-C$_n$ simulations is in consonance with previous experimental and computational results obtained in related systems. Thus, NMR spectroscopy and ITC measurements in different covalently-bound CD dimers (*i.e.* triazole-containing bridged β-CD dimers, and an alkyl altro-α-CD dimer) have confirmed that the CD-CD linker becomes deeply included within the CD cavity thanks to the tumbling (*i.e.* 360° rotation) of one of the monosubstituted glucopyranose units. [77,78] The tumbling is strongly dependent on the spacer nature, it occurs exclusively in water, and it results in a limited accessibility to the CD cavities. Computer simulations performed for the alkyl altro-α-CD further confirmed that the self-inclusion complex is the most stable state in aqueous solution. In addition, the simulations also showed that the tumbling process also stems from the hydrophobicity of the side chain and the propensity of the altro-α-CD derivative to include the alkyl side chain [79].

The complexing capabilities of cyclodextrins for partially hydrophobic guests explain their versatile use as carriers in multiple applications. In the CD-bound complexes, the guest is usually included within the CD cavity primary due to favorable hydrophobic interactions. Our simulations of the β-CD/Dzp complex provide now a detailed molecular picture of the host–guest binding mode, showing that Dzp binds preferentially through the wide rim (*i.e.* the head) of the β-CD molecule, with the unsubstituted phenyl group predominantly included within the hydrophobic cavity of the host. This β-CD/Dzp complex results in a favorable binding free energy (-6.2 kcal/mol) that is in very good agreement with the standard ΔG value obtained from solubility measurements (-5.7 kcal/mol) [24]. In addition, the preferred binding mode with the Phe group included in the cavity is compatible with former solid-state ^{1}H NMR results [26]. According to temperature dependences of spin–lattice relaxation times, the energy barrier for the reorientation of the methyl group *N*-bound to the central 1,4-diazepine ring of Dzp is unaffected by its binding to β-CD. Simple molecular modeling calculations of the host/guess interaction energies considering three different binding modes also conclude that the phenyl ring of Dzp preferentially enters into the β-CD cavity [26].

In principle, amphiphilic CD derivatives have been developed to improve their performance as drug delivery systems. The alkyl substituents in the β-CD-C$_n$ molecules are expected to improve guest complexation by cavity extension or by inducing guest interactions with the alkyl side chains around the torus. However, these alkyl groups also increase the steric hindrance for guest inclusion, and the formation of self-inclusion complexes (*i.e.* with the C$_n$ side chains included in the cavity) clearly compete with guest binding. The MD simulations yield new insight into these effects. On one hand, the alkyl side chains bound at the head of the β-CD ring are found to destabilize the binding of diazepam at the narrow rim due to their self-inclusion through the wide rim. Considering the guest binding at the head of the β-CD ring, the grafted chain length influences the structure and stability of each particular β-CD-C$_n$/Dzp complex. The guest oscillates between fully and partially included configurations when it binds to β-CD-C$_4$, while it is displaced from the cavity and it ends entangled in the aliphatic chains of β-CD-C$_{10}$. Finally, the β-CD-C$_{14}$/Dzp inclusion complex remains stable because the long and flexible C$_{14}$ side chains allow the placement of the Dzp polar groups close to secondary alcohols or solvent molecules and it would be thermodynamically favored. The simulations also show that the largest alkyl side chains (*i.e.* C$_{10}$ and C$_{14}$) impede the inclusion of Dzp through the wide rim. Only the shortest C$_4$ fragment allows the easy entering of the guest through the wide rim during the 5.0 μs-long simulation.

Our simulations reveal that, compared to the unsubstituted β-CD, the binding of Dzp to the amphiphilic β-CD-C$_n$ molecules to form 1:1 complexes is not improved, but deteriorated due to weaker interactions and a less favorable solvation term. Unfortunately, we lack direct experimental evidences confirming the existence and stability of individual β-CD-C$_n$/Dzp complexes. In related systems, previous studies have demonstrated the existence of

inclusion complexes between amphiphilic CD derivatives and various substances [80–82]. In these complexes, the drug is included within the CD cavity or entangled within the "skirt" region comprising the long acyl chains, what seems in agreement with the variety of binding modes observed in our models. The experimental studies also indicate that drug inclusion may be facilitated by leaving the secondary face (*i.e.* head) of the CDs unmodified or with a low degree of substitution. This structural feature is not fulfilled by the examined β-CD-C_n systems that bear full substitution on the O2 hydroxyl groups and, therefore, the formation of inclusion complexes within the β-CD-C_n is affected by steric hindrance and partial closure of the wide side of the cavity as observed during the MD simulations.

As mentioned in the Introduction, there are controversial experimental evidences in the literature about the relevance of β-CD dimerization/aggregation in aqueous solution. Former theoretical calculations [14] have reported PMF curves for the dimerization process that exhibit one or two minima, which are around 5.0 kcal/mol depth. However, these PMF curves are derived from a limited amount of sampling (400 ns) and assume an arbitrary one-dimensional coordinate favoring HH-configurations, what may underestimate the entropic penalty for binding. Since the PMF curve is not integrated over the bound/unbound regions and free energy corrections from volume reduction are not calculated, the depth of the PMF minima most likely overestimates the standard ΔG binding energy [83]. Although our DFTB3/PBSA-based ΔG values would likely contain a systematic error of a few kcal/mol, they are less affected from sampling issues and do not depend on any coordinate choice. In our calculations, the most stable β-CD/β-CD trajectory has a relatively large positive ΔG value of 8.8 kcal/mol ($K \sim 10^{-7}$ for the monomer $\leftrightarrow$ dimer equilibrium), which corresponds to a marginal stability for the β-CD dimer. Furthermore, both the spontaneous monomer–dimer transitions and the loose character of the β-CD···β-CD mainly-polar contacts, contrast sharply with the highly-stable binding mode of β-CD with Dzp using equivalent simulation settings, pointing out again that β-CD dimerization is less favorable than the inclusive binding of β-CD with small and rigid guests. Altogether, we conclude that the present results are more in line with the recent NMR experimental results and former observations, which highlight that the monomeric form of β-CD is largely predominant (>99%) [15–17].

Amphiphilic CDs self-assemble to form a variety of supramolecular structures with applications in controlled drug release [21]. Previous results have shown that the trend to aggregate and the final configuration of the supramolecular assembly depend on the length of the grafted side chains. Interestingly, nanostructures formed by β-CD-C_4 molecules are not detected using the solvent displacement technique, but β-CD-C_n molecules with longer alkyl side chains (C_6-C_{14}) lead to measurable nanoparticles [39]. In addition, imaging techniques reveal that, while the short-chained β-CD-C_6 forms dense nanoparticles that do not exhibit any regular molecular structure [38], β-CD-C_{10} self-organizes into bilayers forming an onion-like structure, and β-CD-C_{14} gives complex faceted nanoparticles with a columnar inverse hexagonal structure [20].

The dimerization of the β-CD-C_n molecules, which represents an elementary first step in their aggregation process, has been carefully characterized in this work. In line with the above experimental observations, we find that the length of the side chain strongly determines both the preferred arrangements and the stability of the dimers. Most remarkably, the simulations and energy calculations discriminate between β-CD-C_4 and β-CD-C_{10}/β-CD-C_{14}. On one hand, the β-CD-C_4/β-CD-C_4 structures produced by the MD simulations resemble those of β-CD as they have abundant CD···CD polar contacts and are quite flexible, adopting various HH-type arrangements and experiencing dissociation events during the

5.0 μs simulations. The lowest ΔG scoring, 11.5 kcal/mol, is not compatible with a significant dimer formation. Therefore, we note that β-CD-C_4 and the parent β-CD molecules share the same lack of affinity for dimer association, what is agreement with the fact that β-CD-C_4 nanoparticles are not detected. On the other hand, the MD models for the β-CD-C_{10} and β-CD-C_{14} dimers unveil the important role played by the hydrophobic packaging of the long alkyl chains favoring more compact dimer structures. For the β-CD-C_{10} system, the dimeric structures may adopt several V-type HH configurations and the estimated ΔG scoring for dimerization ($\sim$0 kcal/mol) suggests that a mixture of monomer and dimer structures could be possible in diluted solutions. According to the simulations, the longer alkyl chains of the β-CD-C_{14} system have a dramatic impact on the structure and stability of the dimers, resulting in compact bilayer-type complexes with nearly-extended and intertwined aliphatic chains, which are thermodynamically much more stable than the separated monomers. Overall, the predicted dimer structure and stability for β-CD-C_{10} and β-CD-C_{14} are clearly in consonance with the affinity of these amphiphilic CDs to aggregate into nanoparticles. We also think that the observed structural differences in the β-CD-C_n dimers might be related with the different type of nanoparticles experimentally detected. Basing on the moderate guest affinity found in the computational models of the 1:1 β-CD-C_n/Dzp complexes, it seems also plausible that guest capture by the β-CD-C_n aggregates would occur through non-inclusive binding modes, especially for β-CD-C_{10}.

Finally, it may be interesting to note that the extensive MD simulations of the isolated amphiphilic CDs and their 1:1 complexes provide useful data about the intrinsic properties of these molecules that are hardly accessible by experimental means due to the spontaneous formation of aggregates at low concentrations. In this way, the analysis of the relative trends derived from the computer models may result in design principles useful to optimize the properties of the amphiphilic derivatives of CDs.

4. Summary and conclusions

Extended MD simulations combined with DFTB3/PBSA and entropy calculations yield valuable data to understand the complexation and aggregation capabilities of selected amphiphilic derivatives of β-CD with aliphatic side chains ester-bound to the secondary O2 alcohols at the wide rim. In aqueous solution, the C_n alkyl side chains in the isolated β-CD-C_n molecules tend to be included within the hydrophobic cavity of the β-CD ring, a behavior previously observed in different CD dimers connected by a covalent linker. Depending on the length of the C_n chains, their self-inclusion behavior modifies the conformation and flexibility of the β-CD ring and the accessibility of its central cavity. Considering diazepam as a typical guess, the simulations confirm the existence of stable β-CD/Dzp inclusion complexes where Dzp preferentially binds at the head of β-CD with its Phe ring located inside the hydrophobic cavity. However, the presence of the alkyl side chains in the selected β-CD-C_n molecules disfavors the formation of inclusion complexes with Dzp. With the shortest C_4 chain, the guest fluctuates between an included and a partially excluded position at the head of the ring, and the binding free energy is significantly reduced compared to the native β-CD. With the largest C_{14} side chain, the β-CD-C_{14}/Dzp inclusion complex with the drug bound at the head remains stable, but the long alkyl side chains at the head of the β-CD ring hinders guest inclusion. Concerning host dimerization, the length of the alkyl side chains determines the conformation and stability of the β-CD-C_n/β-CD-C_n dimers. Increasing the size of the C_n moieties enhances the stability of the dimers and favors a head-to head orientation of the β-CD-C_n rings driven by the hydrophobic packaging of the side chains.

The simulations point out that the bilayer structure obtained for the β-CD-C$_{14}$/β-CD-C$_{14}$ dimer is particularly stable and that the β-CD-C$_4$ and β-CD molecules can hardly aggregate to form stable dimers.

Declaration of Competing Interest

The authors declare that they have no known competing financial interests or personal relationships that could have appeared to influence the work reported in this paper.

Appendix A. Supplementary material

Table S1 with a description of the systems considered in this work. Fig. S1 with histograms for the φ and Ψ angles; Fig. S2 and Table S2 with cluster results; Figs. S3 and S9 with the molecular surface of C$_n$ fragments; Fig. S4 with the initial structures of the β-CD/Dzp complexes; Figs. S5, S7, and S10 with distances and Euler angles; Figs. S6, S8, and S14 with structures extracted from the simulations; Fig. S11 with contact surface area; Fig. S12 with contour maps for the φ and Ψ angles; Fig. S13 with histograms for θ angle; Fig. S15 with histograms for r_{acc}. Tables S3, S4 and S6 with information of contacts with solvent molecules. Table S5 with different energy contributions to β-CD/Dzp binding energies. Zip file containing Dzp and β-CD-C$_n$ parameters.

Supplementary data to this article can be found online at https://doi.org/10.1016/j.molliq.2021.118457.

References

[1] H. Dodziuk, in: H. Dodziuk (Ed.), Cyclodextrins and Their Complexes: Chemistry, Analytical Methods, Applications, Wiley-VCH, Weinheim, 2006, doi: 10.1002/3527608982.

[2] J.-Y. Li, D.-F. Sun, A.-Y. Hao, H.-Y. Sun, J. Shen, Crystal structure of a new cyclomaltoheptaose hydrate: β-cyclodextrin 7.5H$_2$O, Carbohydr. Res. 345 (2010) 685–688, https://doi.org/10.1016/j.carres.2009.12.016.

[3] J. Thaning, B. Stevensson, J. Östervall, K.J. Naidoo, G. Widmalm, A. Maliniak, NMR studies of molecular sonformations in α-cyclodextrin, J. Phys. Chem. B 112 (2008) 8433–8436, https://doi.org/10.1021/jp802681z.

[4] D. Suárez, N. Díaz, Conformational and entropy analyses of extended molecular dynamics simulations of α-, β- and γ-cyclodextrins and of the β-cyclodextrin/nabumetone complex, Phys. Chem. Chem. Phys. 19 (2017) 1431–1440, https://doi.org/10.1039/c6cp06107a.

[5] E.M.M. Del Valle, Cyclodextrins and their uses: a review, Process Biochem. 39 (9) (2004) 1033–1046, https://doi.org/10.1016/S0032-9592(03)00258-9.

[6] A. Rasheed, A. Kumar, V.V.N.S.S. Sravanthi, Cyclodextrins as drug carrier molecule: a review, Sci. Pharm. 76 (4) (2008) 567–598.

[7] S.S. Jambhekar, P. Breen, Cyclodextrins in pharmaceutical formulations i: Structure and physicochemical properties, formation of complexes, and types of complex, Drug Discovery Today 21 (2) (2016) 356–362, https://doi.org/10.1016/j.drudis.2015.11.017.

[8] Z. Bikádi, R. Kurdi, S. Balogh, J. Szemán, E. Hazai, Aggregation of cyclodextrins as an important factor to determine their complexation behavior, Chem. Biodivers. 3 (11) (2006) 1266–1278, https://doi.org/10.1002/cbdv.200690129.

[9] T.F.G.G. Cova, S.M.A. Cruz, A.J.M. Valente, P.E. Abreu, J.M.C. Marques, A.A.C.C. Pais, in: P. Arora (Ed.), Cyclodextrin. A Versatile Ingredient, 2018.

[10] A.W. Coleman, I. Nicolis, N. Keller, J.P. Dalbiez, Aggregation of cyclodextrins: An explanation of the abnormal solubility of β-cyclodextrin, J. Inclusion Phenom. Mol. Recognit. Chem. 13 (2) (1992) 139–143, https://doi.org/10.1007/BF01053637.

[11] M. Bonini, S. Rossi, G. Karlsson, M. Almgren, P. Lo Nostro, P. Baglioni, Self-assembly of β-cyclodextrin in water. Part 1: Cryo-TEM and dynamic and static light scattering, Langmuir 22 (2006) 1478–1484, https://doi.org/10.1021/la052878f.

[12] T. Loftsson, P. Saokham, A. Rodrigues Sá Couto, Self-association of cyclodextrins and cyclodextrin complexes in aqueous solutions, Int. J. Pharm. 560 (2019) 228–234, doi: 10.1016/j.ijpharm.2019.02.004.

[13] A. Ryzhakov, T. Do Thi, J. Stappaerts, L. Bertoletti, K. Kimpe, A.R. Sá Couto, P. Saokham, G. Van den Mooter, P. Augustijns, G.W. Somsen, S. Kurkov, S.

[14] Inghelbrecht, A. Arien, M.I. Jimidar, K. Schrijnemakers, T. Loftsson, Self-assembly of cyclodextrins and their complexes in aqueous solutions, J. Pharm. Sci. 105 (9) (2016) 2556–2569, https://doi.org/10.1016/j.xphs.2016.01.019.

[14] H. Zhang, T. Tan, W. Feng, D. van der Spoel, Molecular recognition in different environments: β-cyclodextrin dimer formation in organic solvents, J. Phys. Chem. B 116 (2012) 12884–112693, https://doi.org/10.1021/jp308416p.

[15] A. Wu, X. Shen, Y. He, Investigation on γ-cyclodextrin nanotube induced by n, n′-diphenylbenzidine molecule, J. Colloid Interface Sci. 297 (2006) 525–533, https://doi.org/10.1016/j.jcis.2005.11.014.

[16] A.J.M. Valente, R.A. Carvalho, O. Söderman, Do cyclodextrins aggregate in water? Insights from NMR experiments, Langmuir 31 (23) (2015) 6314–6320, https://doi.org/10.1021/acs.langmuir.5b01493.

[17] A.J.M. Valente, R.A. Carvalho, D. Murtinho, O. Söderman, Molecular dynamics of cyclodextrins in water solutions from NMR deuterium relaxation: implications for cyclodextrin aggregation, Langmuir 33 (33) (2017) 8233–8238, https://doi.org/10.1021/acs.langmuir.7b01923.

[18] G. Varan, C. Varan, N. Erdoğar, A.A. Hıncal, E. Bilensoy, Amphiphilic cyclodextrin nanoparticles, Int. J. Pharm. 531 (2) (2017) 457–469, https://doi.org/10.1016/j.ijpharm.2017.06.010.

[19] E. Memisoglu, A. Bochot, M. Sen, D. Duchêne, A.A. Hıncal, Non-surfactant nanospheres of progesterone inclusion complexes with amphiphilic β-cyclodextrins, Int. J. Pharm. 251 (2003) 143–153, https://doi.org/10.1016/S0378-5173(02)00593-8.

[20] J.-L. Putaux, C. Lancelon-Pin, F.-X. Legrand, M. Pastrello, L. Choisnard, A. Gèze, C. Rochas, D. Wouessidjewe, Self-assembly of amphiphilic biotransesterified β-cyclodextrins: Supramolecular structure of nanoparticles and surface properties, Langmuir 33 (32) (2017) 7917–7928, https://doi.org/10.1021/acs.langmuir.7b01136.

[21] V. Bonnet, C. Gervaise, F. Djedaïni-Pilard, A. Furlan, C. Sarazin, Cyclodextrin nanoassemblies: a promising tool for drug delivery, Drug Discovery Today 20 (9) (2015) 1120–1126, https://doi.org/10.1016/j.drudis.2015.05.008.

[22] C. Holvoet, Y. Vander Heyden, J. Plaizier-Vercammen, Inclusion complexation of diazepam with different cyclodextrins in formulations for parenteral use, Pharmazie 60 (2005) 598–603.

[23] K. Hajnal, G. Hancu, D.L. Muntean, J.P. Cusu, Optimization of diazepam solubility with auxiliary substances and thermo analytical investigation of binary systems, Rev. Chim. 67 (2016) 2065–2070.

[24] M.V. Rekharsky, Y. Inoue, Complexation thermodynamics of cyclodextrins, Chem. Rev. 98 (5) (1998) 1875–1918, https://doi.org/10.1021/cr970015o.

[25] K. Cai, J. Li, Z. Luo, Y. Hu, Y. Hou, X. Ding, β-cyclodextrin conjugated magnetic nanoparticles for diazepam removal from blood, Chem. Commun. 47 (2011) 7719–7721, https://doi.org/10.1039/C1CC11855B.

[26] A. Pajzderska, J. Mielcarek, J. Wasicki, Complex and mixture of β-cyclodextrin with diazepam characterised by ^{1}H NMR and atom–atom potential methods, Carbohydr. Res. 398 (2014) 56–62, https://doi.org/10.1016/j.carres.2014.07.025.

[27] A. Gèze, L. Choisnard, J.-L. Putaux, D. Wouessidjewe, Colloidal systems made of biotransesterified α, β and γ cyclodextrins grafted with C10 alkyl chains, Mater. Sci. Eng., C 29 (2) (2009) 458–462, https://doi.org/10.1016/j.msec.2008.08.027.

[28] L. Wickstrom, P. He, E. Gallicchio, R.M. Levy, Large scale affinity calculations of cyclodextrin host-guest complexes: understanding the role of reorganization in the molecular recognition process, J. Chem. Theory Comput. 9 (7) (2013) 3136–3150, https://doi.org/10.1021/ct400003r.

[29] H. Zhang, C. Yin, H. Yan, D. van der Spoel, Evaluation of Generalized Born models for large scale affinity prediction of cyclodextrin host–guest complexes, J. Chem. Inf. Model. 56 (10) (2016) 2080–2092, https://doi.org/10.1021/acs.jcim.6b00418.

[30] J. Yin, N.M. Henriksen, D.R. Slochower, M.R. Shirts, M.W. Chiu, D.L. Mobley, M.K. Gilson, Overview of the SAMPl5 host-guest challenge: are we doing better?, J Comput. Aided Mol. Des. 31 (1) (2017) 1–19, https://doi.org/10.1007/s10822-016-9974-4.

[31] N.M. Henriksen, M.K. Gilson, Evaluating force field performance in thermodynamic calculations of cyclodextrin host-guest binding: Water models, partial charges, and host force field parameters, J. Chem. Theory Comput. 13 (9) (2017) 4253–4269, https://doi.org/10.1021/acs.jctc.7b00359.

[32] Z. Tang, C.A. Chang, Binding thermodynamics and kinetics calculations using chemical host and guest: a comprehensive picture of molecular recognition, J. Chem. Theory Comput. 14 (1) (2018) 303–318, https://doi.org/10.1021/acs.jctc.7b00899.

[33] D. Suárez, N. Díaz, Affinity calculations of cyclodextrin host−guest complexes: assessment of strengths and weaknesses of end-point free energy methods, J. Chem. Inf. Model. 59 (1) (2019) 421–440, https://doi.org/10.1021/acs.jcim.8b00805.

[34] T.F. Cova, B.F. Milne, A.A.C.C. Pais, Host flexibility and space filling in supramolecular complexation of cyclodextrins: a free-energy-oriented approach, Carbohydr. Polym. 205 (2019) 42–54, https://doi.org/10.1016/j.carbpol.2018.10.009.

[35] K. Lindner, W. Saenger, Crystal and molecular structure of cyclohepta-amylose dodecahydrate, Carbohydr. Res. 99 (2) (1982) 103–115, https://doi.org/10.1016/S0008-6215(00)81901-1.

[36] R. Salomon-Ferrer, D.A. Case, R.C. Walker, An overview of the Amber biomolecular simulation package, WIREs Comput. Mol. Sci. 3 (2) (2013) 198–210, https://doi.org/10.1002/wcms.1121.

[37] D.A. Case, I.Y. Ben-Shalom, S.R. Brozell, D.S. Cerutti, I. Cheatham, T.E. , V.W.D. Cruzeiro, T.A. Darden, R.E. Duke, D. Ghoreishi, M.K. Gilson, H. Gohlke, A.W.

Goetz, D. Greene, R. Harris, N. Homeyer, S. Izadi, A. Kovalenko, T. Kurtzman, T. S. Lee, S. LeGrand, P. Li, C. Lin, J. Liu, T. Luchko, R. Luo, D.J. Mermelstein, K.M. Merz, Y. Miao, G. Monard, C. Nguyen, H. Nguyen, I. Omelyan, A. Onufriev, F. Pan, R. Qi, D.R. Roe, A. Roitberg, C. Sagui, S. Schott-Verdugo, J. Shen, C.L. Simmerling, J. Smith, R. Salomon-Ferrer, J. Swails, R.C. Walker, J. Wang, H. Wei, R.M. Wolf, X. Wu, L. Xiao, D.M. York, P.A. Kollman, University of California, San Francisco, 2018.

[38] L. Choisnard, A. Gèze, J.-L. Putaux, Y.-S. Wong, D. Wouessidjewe, Nanoparticles of β-cyclodextrin esters obtained by self-assembling of biotransesterified β-cyclodextrins, Biomacromolecules 7 (2006) 515–520, https://doi.org/10.1021/bm0507655.

[39] L. Choisnard, A. Gèze, B.G.J. Yaméogo, J.-L. Putaux, D. Wouessidjewe, Miscellaneous nanoaggregates made of β-CD esters synthesised by an enzymatic pathway, Int. J. Pharm. 344 (1-2) (2007) 26–32, https://doi.org/10.1016/j.ijpharm.2007.06.026.

[40] M.J. Frisch, G.W. Trucks, H.B. Schlegel, G.E. Scuseria, M.A. Robb, J.R. Cheeseman, G. Scalmani, V. Barone, B. Mennucci, G.A. Petersson, H. Nakatsuji, M. Caricato, X. Li, H.P. Hratchian, A.F. Izmaylov, J. Bloino, G. Zheng, J.L. Sonnenberg, M. Hada, M. Ehara, K. Toyota, R. Fukuda, J. Hasegawa, M. Ishida, T. Nakajima, Y. Honda, O. Kitao, H. Nakai, T. Vreven, J.A. Montgomery Jr., J.E. Peralta, F. Ogliaro, M.J. Bearpark, J. Heyd, E.N. Brothers, K.N. Kudin, V.N. Staroverov, R. Kobayashi, J. Normand, K. Raghavachari, A.P. Rendell, J.C. Burant, S.S. Iyengar, J. Tomasi, M. Cossi, N. Rega, N.J. Millam, M. Klene, J.E. Knox, J.B. Cross, V. Bakken, C. Adamo, J. Jaramillo, R. Gomperts, R.E. Stratmann, O. Yazyev, A.J. Austin, R. Cammi, C. Pomelli, J.W. Ochterski, R.L. Martin, K. Morokuma, V.G. Zakrzewski, G.A. Voth, P. Salvador, J.J. Dannenberg, S. Dapprich, A.D. Daniels, Ö. Farkas, J.B. Foresman, J.V. Ortiz, J. Cioslowski, D.J. Fox, Gaussian, Inc., Wallingford, CT, USA, 2009.

[41] F. Jensen, Introduction to Computational Chemistry, third ed., John Wiley, 2017.

[42] K.N. Kirschner, A.B. Yongye, S.M. Tschampel, J. González-Outeiriño, C.R. Daniels, B.L. Foley, R.J. Woods, Glycam06: a generalizable biomolecular force field, Carbohydr. J. Comput. Chem. 29 (4) (2008) 622–655, https://doi.org/10.1002/jcc.20820.

[43] C.I. Bayly, P. Cieplak, W. Cornell, P.A. Kollman, A well-behaved electrostatic potential based method using charge restraints for deriving atomic charges: the RESP model, J. Phys. Chem. 97 (40) (1993) 10269–10280, https://doi.org/10.1021/j100142a004.

[44] A.S. Dayananda, H.S. Yathirajan, T. Gerber, E. Hosten, R. Betz, Redetermination of the structure of 7-chloro-1,3-dihydro-1-methyl-5-phenyl-1,4-benzodiazepin-2(3H)-one, $C_{16}H_{13}ClN_2O$, Zeitschrift für Kristallographie - New Cryst. Struct. 228 (2013) 223–224, https://doi.org/10.1524/ncrs.2013.0111.

[45] J. Wang, R.M. Wolf, J.W. Caldwell, P.A. Kollman, D.A. Case, Development and testing of a general Amber force field, J. Comput. Chem. 25 (9) (2004) 1157–1174, https://doi.org/10.1002/jcc.20035.

[46] R.M. Betz, R.C. Walker, Paramfit: automated optimization of force field parameters for molecular dynamics simulations, J. Comput. Chem. 36 (2) (2015) 79–87, https://doi.org/10.1002/jcc.23775.

[47] D. Sheppard, R. Terrell, G. Henkelman, Optimization methods for finding minimum energy paths, J. Chem. Phys. 128 (13) (2008) 134106, https://doi.org/10.1063/1.2841941.

[48] F. Neese, The ORCA program system, WIREs Comput. Mol. Sci. 2 (1) (2012) 73–78, https://doi.org/10.1002/wcms.81.

[49] S. Grimme, A. Hansen, J.G. Brandenburg, C. Bannwarth, Dispersion-corrected mean-field electronic structure methods, Chem. Rev. 116 (9) (2016) 5105–5154, https://doi.org/10.1021/acs.chemrev.5b00533.

[50] K. Ramig, E.M. Greer, D.J. Szalda, S. Karimi, A. Ko, L. Boulos, J. Gu, N. Dvorkin, H. Bhramdat, G. Subramaniam, NMR spectroscopic and computational study of conformational isomerism in substituted 2-aryl-3H-1-benzazepines: toward isolable atropisomeric benzazepine enantiomers, J. Org. Chem. 78 (16) (2013) 8028–8036, https://doi.org/10.1021/jo4013089.

[51] W.L. Jorgensen, J. Chandrasekhar, J.D. Madura, R.W. Impey, M.L. Klein, Comparison of simple potential functions for simulating liquid water, J. Chem. Phys. 79 (2) (1983) 926–935, https://doi.org/10.1063/1.445869.

[52] A.R. Leach, Molecular Modelling: Principles and Applications, Pearson, 2001.

[53] U. Essmann, L. Perera, M.L. Berkowitz, T. Darden, H. Lee, L.G. Pedersen, A smooth particle mesh ewald method, J. Chem. Phys. 103 (19) (1995) 8577–8593, https://doi.org/10.1063/1.470117.

[54] R. Salomon-Ferrer, A.W. Götz, D. Poole, S. Le Grand, R.C. Walker, Routine microsecond molecular dynamics simulations with Amber on GPUs. 2. Explicit solvent particle mesh ewald, J. Chem. Theory Comput. 9 (9) (2013) 3878–3888, https://doi.org/10.1021/ct400314y.

[55] S. Le Grand, A.W. Götz, R.C. Walker, SPFP: speed without compromise-A mixed precision model for GPU accelerated molecular dynamics simulations, Comput. Phys. Commun. 184 (2) (2013) 374–380, https://doi.org/10.1016/j.cpc.2012.09.022.

[56] D.R. Roe, T.E. Cheatham, Ptraj and cpptraj: software for processing and analysis of molecular dynamics trajectory data, J. Chem. Theory Comput. 9 (7) (2013) 3084–3095, https://doi.org/10.1021/ct400341p.

[57] J. Weiser, P.S. Shenkin, W.C. Still, Approximate solvent-accessible surface areas from tetrahedrally directed neighbor densities, Biopolymers 50 (1999) 373–380, https://doi.org/10.1002/(SICI)1097-0282(19991005)50:4<373::AID-BIP3>3.0.CO;2-U.

[58] E.F. Pettersen, T.D. Goddard, C.C. Huang, G.S. Couch, D.M. Greenblatt, E.C. Meng, T.E. Ferrin, UCSF chimera-A visualization system for exploratory research and analysis, J. Comput. Chem. 25 (13) (2004) 1605–1612, https://doi.org/10.1002/jcc.20084.

[59] M.F. Sanner, J.-C. Spehner, A.J. Olson, Reduced surface: an efficient way to compute molecular surfaces, Biopolymers 38 (1996) 305–320, https://doi.org/10.1002/(SICI)1097-0282(199603)38:3<305::AID-BIP4>3.0.CO;2-Y.

[60] N. Diaz, D. Suarez, Molecular dynamics simulations of matrix metalloproteinase 2: role of the structural metal ions, Biochemistry 46 (2007) 8943–8952, https://doi.org/10.1021/bi700541p.

[61] M. Elstner, D. Porezag, G. Jungnickel, J. Elsner, M. Haugk, T. Frauenheim, S. Suhai, G. Seifert, Self-consistent-charge density-functional tight-binding method for simulations of complex materials properties, Phys. Rev. B 58 (11) (1998) 7260–7268.

[62] T. Krüger, M. Elstner, P. Schiffels, T. Frauenheim, Validation of the density-functional based tight-binding approximation method for the calculation of reaction energies and other data, J. Chem. Phys. 122 (11) (2005) 114110, https://doi.org/10.1063/1.1871913.

[63] M. Gaus, A. Goez, M. Elstner, Parametrization and benchmark of DFTB3 for organic molecules, J. Chem. Theory Comput. 9 (1) (2013) 338–354, https://doi.org/10.1021/ct300849w.

[64] M. Kubillus, T. Kubař, M. Gaus, J. Řezáč, M. Elstner, Parameterization of the DFTB3 method for Br, Ca, Cl, F, I, K, and Na in organic and biological systems, J. Chem. Theory Comput. 11 (1) (2015) 332–342, https://doi.org/10.1021/ct5009137.

[65] C. Tan, Y.-H. Tan, R. Luo, Implicit nonpolar solvent models, J. Phys. Chem. B 111 (42) (2007) 12263–12274, https://doi.org/10.1021/jp073399n.

[66] A. Pecina, S. Haldar, J. Fanfrlík, R. Meier, J. Řezáč, M. Lepšík, P. Hobza, SQM/COSMO scoring function at the DFTB3-D3H4 level: unique identification of native protein–ligand poses, J. Chem. Inf. Model. 57 (2) (2017) 127–132, https://doi.org/10.1021/acs.jcim.6b00513.

[67] J. Řezáč, Cuby: an integrative framework for computational chemistry, J. Comput. Chem. 37 (13) (2016) 1230–1237, https://doi.org/10.1002/jcc.24312.

[68] M. Karplus, T. Ichiye, B.M. Pettitt, Configurational entropy of native proteins, Biophys. J. 52 (6) (1987) 1083–1085, https://doi.org/10.1016/S0006-3495(87)83303-9.

[69] D. Suárez, N. Díaz, Direct methods for computing single-molecule entropies from molecular simulations, WIREs Comput. Mol. Sci. 5 (1) (2015) 1–26, https://doi.org/10.1002/wcms.1195.

[70] J. Kongsted, U. Ryde, An improved method to predict the entropy term with the MM/PBSA approach, J. Comput. Aided Mol. Des. 23 (2) (2009) 63–71, https://doi.org/10.1007/s10822-008-9238-z.

[71] S. Grimme, Supramolecular binding thermodynamics by dispersion-corrected density functional theory, Chem. Eur. J. 18 (32) (2012) 9955–9964, https://doi.org/10.1002/chem.201200497.

[72] E. Suárez, N. Díaz, J. Méndez, D. Suárez, CENCALC: a computational tool for conformational entropy calculations from molecular simulations, J. Comput. Chem. 34 (23) (2013) 2041–2054, https://doi.org/10.1002/jcc.23350.

[73] E. Suárez, D. Suárez, Multibody local approximation: application to conformational entropy calculations on biomolecules, J. Chem. Phys. 137 (8) (2012) 084115, https://doi.org/10.1063/1.4748104.

[74] F.A. Menard, A physico-chemical study of the complexation of cyclodextrins with phramaceutical substances, University of Rhode Island, 1988, Open Access Dissertations, paper 184. Available from: <https://digitalcommons.uri.edu/oa_diss/184>.

[75] S. Genheden, U. Ryde, The MM/PBSA and MM/GBSA methods to estimate ligand-binding affinities, Expert Opin. Drug Discovery 10 (5) (2015) 449–461, https://doi.org/10.1517/17460441.2015.1032936.

[76] C. Wang, D.A. Greene, L. Xiao, R. Qi, R. Luo, Recent developments and applications of the MMPBSA method, Front. Mol. Biosci. 4 (2018), https://doi.org/10.3389/fmolb.2017.00087.

[77] K. Yamauchi, A. Miyawaki, Y. Takashima, H. Yamaguchi, A. Harada, Switching from altro-α-cyclodextrin dimer to pseudo[1]rotaxane dimer through tumbling, Org. Lett. 12 (6) (2010) 1284–1286, https://doi.org/10.1021/ol1001736.

[78] S. Menuel, N. Azaroual, D. Landy, N. Six, F. Hapiot, E. Monflier, Unusual inversion phenomenon of β-cyclodextrin dimers in water, Chem. – A Eur. J. 17 (14) (2011) 3949–3955, https://doi.org/10.1002/chem.201003221.

[79] Y. Liu, C. Chipot, X. Shao, W. Cai, What causes tumbling of altro-α-CD derivatives? Insight from computer simulations, RSC Adv. 5 (71) (2015) 57309–57317, https://doi.org/10.1039/C5RA05642J.

[80] V. Zia, R.A. Rajewski, V.J. Stella, Thermodynamics of binding of neutral molecules to sulfobutyl ether β-cyclodextrins (SBE-β-CDs): the effect of total degree of substitution, Pharm. Res. 17 (2000) 936–941, https://doi.org/10.1023/A:1007571019908.

[81] E. Memişoğlu, A. Bochot, M. Özalp, M. Şen, D. Duchêne, A.A. Hincal, Direct formation of nanospheres from amphiphilic β-cyclodextrin inclusion complexes, Pharm. Res. 20 (2003) 117–125, https://doi.org/10.1023/A:1022263111961.

[82] R. Cavalli, F. Trotta, M. Trotta, L. Pastero, D. Aquilano, Effect of alkylcarbonates of γ-cyclodextrins with different chain lengths on drug complexation and release characteristics, Int. J. Pharm. 339 (1-2) (2007) 197–204, https://doi.org/10.1016/j.ijpharm.2007.03.001.

[83] S. Doudou, N.A. Burton, R.H. Henchman, Standard free energy of binding from a one-dimensional potential of mean force, J. Chem. Theory Comput. 5 (4) (2009) 909–918, https://doi.org/10.1021/ct8002354.